

From simple labels to semantic image segmentation: Leveraging citizen science plant photographs for tree species mapping in drone imagery

Salim Soltani^{1,2,3*}, Olga Ferlian^{3,5}, Nico Eisenhauer^{3,5}, Hannes Feilhauer^{1,2,3,4}, and Teja Kattenborn^{1,3}

¹Remote Sensing Centre for Earth System Research (RSC4Earth), Leipzig University, Germany

²Center for scalable data analytics and artificial intelligence (ScaDS.AI), Leipzig University, Germany

³German Centre for Integrative Biodiversity Research (iDiv), Halle-Jena-Leipzig, Germany

⁴Helmholtz Centre for Environmental Research, Leipzig, Germany

⁵Institute of Biology, Leipzig University, Germany

* Corresponding author: salim.soltani@uni-leipzig.de

Abstract

Knowledge of plant species distributions is essential for various application fields, such as nature conservation, agriculture, and forestry. Remote sensing data, especially high-resolution orthoimages from Unoccupied Aerial Vehicles (UAVs), paired with novel pattern recognition methods, such as Convolutional Neural Networks (CNNs), enable an accurate mapping (segmentation) of plant species. Training transferable pattern recognition models for species segmentation across diverse landscapes and data characteristics typically requires extensive training data. Training data are usually derived from labor-intensive field surveys or visual interpretation of remote sensing images. Alternatively, pattern recognition models could be trained more efficiently with plant photos and labels from citizen science platforms, which include millions of crowd-sourced smartphone photos and the corresponding species labels. However, these pairs of citizen science-based photographs and simple species labels (one label for the entire image) cannot be used directly for training state-of-the-art segmentation models used for UAV image analysis, which require per-pixel labels for training (also called masks). Here, we overcome the limitation of simple labels of citizen science plant observations with a two-step approach: In the first step, we train CNN-based image classification models using the simple labels and apply them in a moving-window approach over UAV orthoimagery to create segmentation masks. In the second phase, these segmentation masks are used to train state-of-the-art CNN-based image segmentation models with an encoder-decoder structure. We tested the approach on UAV orthoimages acquired in summer and autumn on a test site comprising ten temperate deciduous tree species in varying mixtures. Several tree species could be mapped with surprising accuracy (mean F1-score = 0.47). In homogenous species assemblages, the accuracy increased considerably (mean F1-score 0.55). The results indicate that several tree species can be mapped without generating new training data, by but only using pre-existing knowledge from citizen science. Moreover, our analysis revealed that citizen

27 science photographs’ variability in acquisition data and context facilitates the generation
28 of models that are transferable through the vegetation season. Thus, citizen science data
29 may greatly advance our capacity to monitor hundreds of plant species and, thus, Earth’s
30 biodiversity across space and time.

31 Keywords: Remote Sensing, Convolutional Neural Network, Citizen Science Data,
32 Plant species, Transfer learning.

33 1 Introduction

34 Spatially explicit information on plant species is crucial for various domains and application,
35 including nature conservation, agriculture, and forestry. For instance, species information
36 is required for the identification of threatened or invasive species, the location of weeds or
37 crops in precision farming, or tree species classification for forest inventories. Remote sensing
38 emerged as a promising tool for mapping plant species (Müllerová et al., 2023; Bouguettaya
39 et al., 2022; Fassnacht et al., 2016). Thereby, supervised machine learning algorithms are
40 commonly used to identify species-specific features in spatial, temporal, or spectral patterns
41 of remotely sensed signals (Sun et al., 2021; Maes and Steppe, 2019; Lopatin et al., 2019;
42 Curnick et al., 2021; Wagner, 2021). In recent years, remote sensing imagery from drones,
43 also known as Unoccupied Air Vehicles (UAVs), has emerged as an effective source of infor-
44 mation for mapping plant species (Kattenborn et al., 2021; Fassnacht et al., 2016; Schiefer
45 et al., 2020). By means of mosaicing a series of individual image frames, UAVs enable the
46 creation of georeferenced orthoimagery of relatively large areas with extremely high spatial
47 resolution, e.g., in the mili- or centimeter range. The fine spatial grain of such imagery can
48 reveal distinctive morphological plant features to identify specific plant species. Such plant
49 features include the leaf shape, flowers, branching patterns, or crown structures (Sun et al.,
50 2021; Kattenborn et al., 2019a). An effective way to harness this spatial detail is provided
51 by deep learning-based pattern-recognition techniques, in particular by Convolutional Neural
52 Networks (CNN). A series of studies have demonstrated that CNN allows to precisely seg-
53 ment plant species’ canopies in high-resolution UAV imagery (Kattenborn et al., 2021; Hoesser
54 and Kuenzer, 2020; Brodrick et al., 2019). Such CNN models learn the characteristic spatial
55 features of the target (here, plant species) through a cascade of filter operations (convolu-
56 tions). Given these high-dimensional computations, efficiently adopting these models to UAV
57 orthoimagery, which often have large spatial extents and high resolution, requires training
58 and applying them sequentially using smaller sub-regions of an orthoimage (e.g., image tiles
59 of 512 by 512 pixels, Fig. 1c).

60 However, generating models that are transferable across various landscapes and remote
61 sensing data characteristics requires large amounts of training data (Kattenborn et al., 2021;
62 Galuszynski et al., 2022). In particular, when neighboring plant species bear a resemblance, a
63 wealth of training data becomes essential, allowing the model to discern the subtle distinctions
64 between these species (Kattenborn et al., 2021; Schiefer et al., 2020). Commonly, the genera-
65 tion of training data is costly, as training data are usually derived from field surveys or visual
66 interpretation of remote sensing images, also known as annotation or labelling. Both methods

67 have limitations: Field surveys are often logistically challenged by site accessibility or travel
68 costs. Moreover, field surveys commonly only enable the acquisition of point observations or
69 relative cover fractions of the target species (Leitão et al., 2018). Visual image interpretation
70 is often much more effective (Kattenborn et al., 2019b; Schiefer et al., 2023) but for some
71 species, precise visual identification of species can be challenging due to subtle indicative
72 morphological features, the variability of these features in the landscape, or the complexity of
73 vegetation communities (e.g., smooth transitions of canopies of different species). Moreover,
74 the representativeness of data derived from field surveys and visual interpretation is often
75 limited to the location where and when the data were acquired. This can reduce a model’s
76 generalization to new regions or time periods (Cloutier et al., 2023; Kattenborn et al., 2022).
77 Therefore, the obtained amount and quality of training data can be a critical factor for the
78 performance and transferability of CNN models (Bayraktar et al., 2020; Rzanny et al., 2019;
79 Brandt et al., 2020).

80 The challenge of limited training data for UAV-based plant species identification may
81 be alleviated by the collective power of scientists and citizens openly sharing their plant
82 observations on the web (Ivanova and Shashkov, 2021; Fraisl et al., 2022; Di Cecco et al.,
83 2021). A particular data treasure in this regard is generated by citizen science projects
84 for plant species identification. Examples are the iNaturalist and Pl@ntNet projects, which
85 encourage ten-thousands of individuals to capture, share, and annotate photographs of the
86 World’s plant life (Boone and Basille, 2019; Di Cecco et al., 2021). The quantity of such
87 citizen science observations is rapidly growing due to the increasing number of volunteers
88 participating in such projects (Boone and Basille, 2019; Di Cecco et al., 2021).

89 Currently, the iNaturalist project contains over 26 mil globally distributed and annotated
90 photographs of vascular plant species. The iNaturalist platform allows users to identify plant
91 species manually or using a computer vision model integrated into the platform. The sub-
92 mitted observations are then evaluated by the community, and a research-grade classification
93 is assigned if over two-thirds of the community agrees on the species identification. The
94 Pl@ntNet project includes over 20 Mio observations of globally distributed vascular plants.
95 Pl@ntNet requires users to photograph their observations and select an organ tag (e.g., leaf,
96 flower, fruit, or stem). Pl@ntNet features an image recognition algorithm to analyze the
97 tagged photograph and suggest a plant species. Pl@ntNet’s validation process uses a dy-
98 namic approach, combining automated algorithm confidence with community consensus (Joly
99 et al., 2016). The validated observations of iNaturalist and Pl@ntNet are shared via the
100 Global Biodiversity Information Facility (GBIF), a global network that provides open access
101 to biodiversity data (GBIF, 2019).

102 Citizen science-based plant photographs with species annotations provide a valuable, large,
103 and continuously growing data source for training pattern recognition models, such as CNNs
104 (Van Horn et al., 2018; Joly et al., 2016). However, such citizen science data has a cardinal
105 limitation: It only provides simple species annotation for a plant photograph (*the image_i*
106 *shows species_j*). Hence, these labels only enable to train image classification models that
107 predict the likelihood of a species being present in an image but not where in the image.

108 Ideally, for species mapping applications, the species labels would delineate the regions or
109 pixels belonging to a species (*The pixels in the right corner of image_i represents species_j*).
110 Such labels (known as masks) could be used to train CNN-based segmentation models, which
111 can predict a species probability for each individual pixel of an image (or tile of an orthoimage)
112 ([Galuszynski et al., 2022](#); [Schiefer et al., 2020](#)).

113 In a pioneering study by [Soltani et al. \(2022\)](#), the limitation of the simple labels that come
114 with citizen science photographs was overcome by a workaround. At first, image classification
115 models were trained with citizen science data and simple labels to predict a species per image.
116 The trained image classification models were then applied sequentially on tiles of UAV-based
117 orthomosaics in a moving-window-like fashion with very high overlap (Fig. 1a). Lastly, the
118 individual predictions derived from the moving-window steps were rasterized to a seamless
119 segmentation map (Fig. 1b). However, this workaround is computationally intense and in-
120 efficient for large or multiple UAV orthomosaics, as segmentation maps can only be derived
121 from many overlapping prediction steps. In contrast, state-of-the-art CNN-based segmenta-
122 tion methods (typically an encoder-decoder structure) used in remote sensing applications are
123 trained with reference data in the form of masks with dimensions (pixels) corresponding to
124 the extent of the input imagery, where each pixel of the mask defines the absence or presence
125 of a class (here plant species) in the imagery ([Kattenborn et al., 2021](#)). Respective segmen-
126 tation models are more efficient as they segment multiple classes in a single prediction step.
127 Moreover, they enable more detailed class representations in situations where multiple classes
128 are arranged in complex patterns.

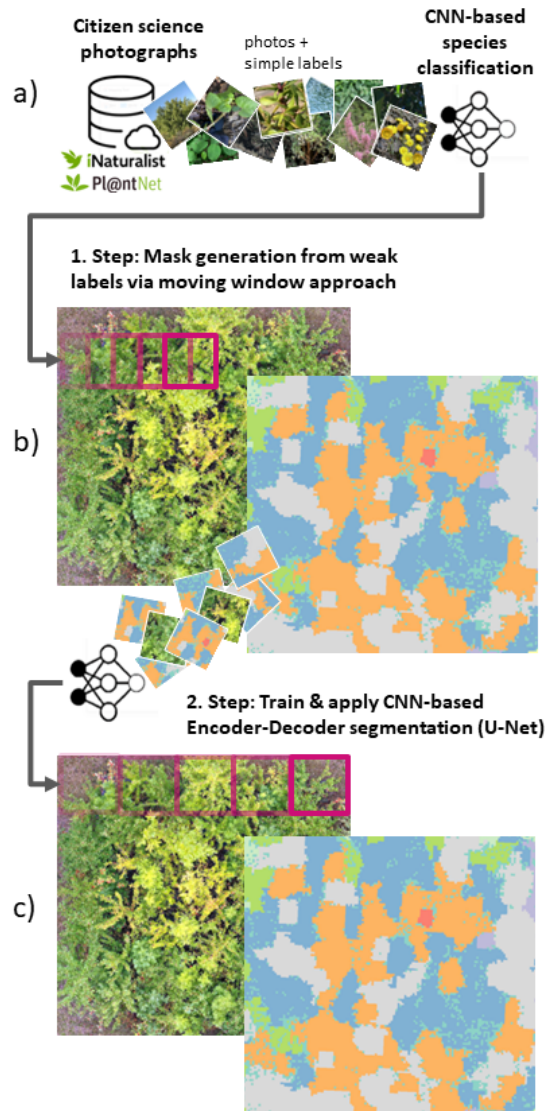


Figure 1: 1-column figure: Schematic representation of the proposed workflow, including the moving window approach by [Soltani et al. \(2022\)](#) (a,b) and the use of state-of-the-art encoder-decoder segmentation algorithms (c).

129 Here, we propose a solution to overcome the limitation of simple annotations of citizen
 130 science plant observations with a two-step approach: In the first step, we apply the procedure
 131 of [Soltani et al. \(2022\)](#), involving CNN-based image classification models trained on citizen
 132 science photographs and simple species labels to predict plant species in UAV orthoimages
 133 using the moving-window approach described above (Fig. 1a, b). Although computationally
 134 demanding, this serves to create segmentation masks for UAV orthoimages. In the second step,
 135 these segmentation masks are used to train more efficient CNN-based image segmentation
 136 models with an encoder-decoder structure (Fig. 1c). These more efficient models could then
 137 be applied to larger spatial extents or to new UAV orthomosaics (e.g. of different sites or
 138 time steps).

139 The present study, hence, addresses the following research questions:

- 140 • Can we harness weak labels from citizen science plant observations to train efficient
141 state-of-the-art semantic segmentation models?
- 142 • Do those segmentation models also increase the accuracy compared to the simple moving
143 window approach?

144 These questions are evaluated on a tree species dataset acquired on an experimental site
145 (MyDiv experiment, Bad Lauchstädt, Germany), where ten temperate deciduous tree species
146 were planted in stratified and complex mixtures. The selection of this location is attributed
147 to its harmonious coexistence of various plant species within a compact area.

148 2 Methods

149 2.1 Data acquisition and pre-processing

150 2.1.1 Study site and drone data acquisition

151 The MyDiv experimental site is located in Bad Lauchstädt, Saxony-Anhalt, Germany (lati-
152 tude, 51°23' N, longitude, 11°53' E). The site comprises 80 plots with different configurations
153 of ten deciduous tree species, including *Acer pseudoplatanus*, *Aesculus hippocastanum*, *Betula*
154 *pendula*, *Carpinus betulus*, *Fagus sylvatica*, *Fraxinus excelsior*, *Prunus avium*, *Quercus petraea*,
155 *Sorbus aucuparia*, and *Tilia platyphyllos* (Ferlian et al., 2018). Each plot measures 12 m by
156 12 m and contains 140 trees planted at distances of 1 m (Fig 2). In total, all plots together
157 accommodate 11,200 individual trees. Each plot contains varying tree species compositions,
158 including one, two, and four tree species. This variety in species, their balanced composition,
159 and plots of different canopy complexity (species mixtures) provide an ideal setting to test
160 the proposed species segmentation approach.

161 We collected UAV-based RGB aerial imagery over the MyDiv experimental site using a
162 DJI Mavic 2 Pro and the flight planning software DroneDeploy (vers. 5.0, USA). Two flights
163 were conducted in 2022 in July and September, where July corresponds to the peak of the
164 growing season and September to the senescence stage (Fig 2). The flight plan was setup
165 with a forward overlap of 90%, side overlap of 70% at an altitude of 16 m (ground sampling
166 distance of approximately 0.22 cm per pixel). We used the generated images and Metashape
167 (vers. 1.7.6, Agisoft LLC) to generate orthoimages for both flight campaigns. The orthoimage
168 for July and September are onward called Ortho_{July} and Ortho_{September}, respectively.

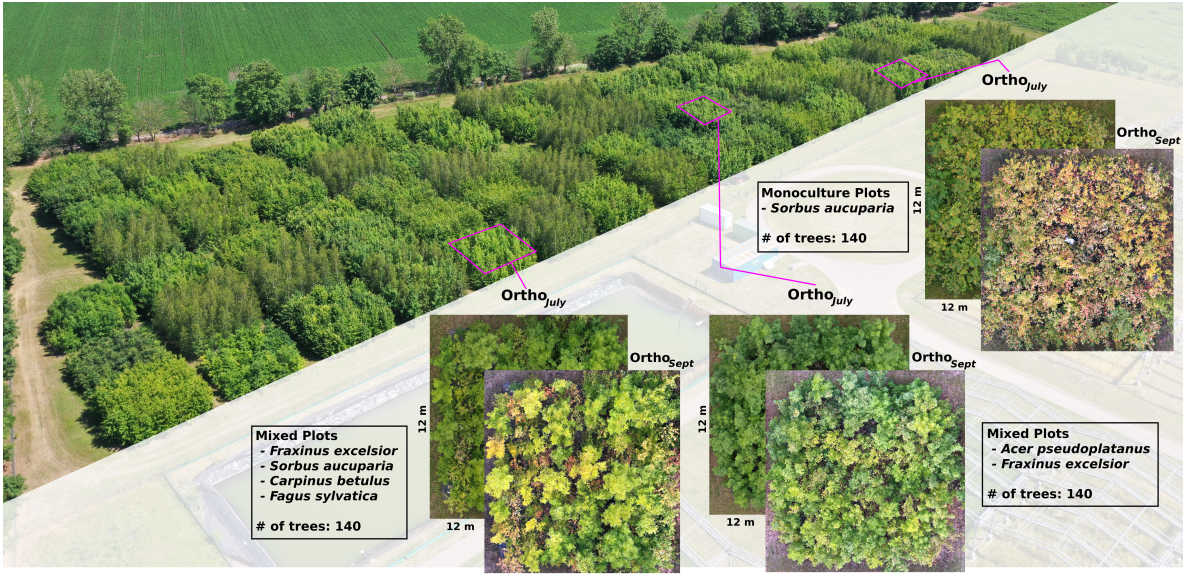


Figure 2: Overview of the MyDiv experimental site with close-ups for three plots of different species composition. The MyDiv site is located at Lat. 51.3916 N, Long. 11.8857 E.

169 To evaluate the performance of the CNN models for tree species mapping, we created
 170 reference data by manually delineating the tree species in the UAV orthoimages in QGIS
 171 (vers. 3.32.3). To reduce the workload, we did not delineate the species for the entire plot
 172 but for diagonal transects with 20 m length and 2 m width.

173 2.1.2 Citizen science training data

174 We queried citizen science plant observations of the iNaturalist and Pl@ntNet datasets via
 175 the GBIF database for our target tree species using scientific names. For the iNaturalist data,
 176 we used the R package rinat (vers. 0.1.8), an API to iNaturalist. The Pl@ntNet data for the
 177 selected tree species were acquired using the tabulated observation data from GBIF and the
 178 integrated URLs to the images. The number of photographs available from iNaturalist and
 179 Pl@ntNet varied for the different tree species. Per species, we were able to acquire between
 180 582 to 10000 photographs (mean 7696) from the iNaturalist dataset and 221 to 3304 images
 181 (mean 2238) from the Pl@ntNet dataset (details see Appendix Table A1).

182 In addition to the tree species, we added a background class to consider canopy gaps
 183 between trees. Training data for this background class was obtained using the Google Image
 184 API and queries of different keywords, e.g. *grass*, *forest floor*, *forest ground*. After cleaning the
 185 obtained images for non-meaningful results, the background class included 1100 photographs.

186 We converted all photographs to a rectangular shape by cropping them to the shorter side
 187 and resampled them to a common size of 512×512 pixels (the tile size used later for the CNN
 188 model generation). Figure 3 shows examples of the downloaded photographs for the different
 189 tree species and a comparison to their appearance in Ortho_{July}.

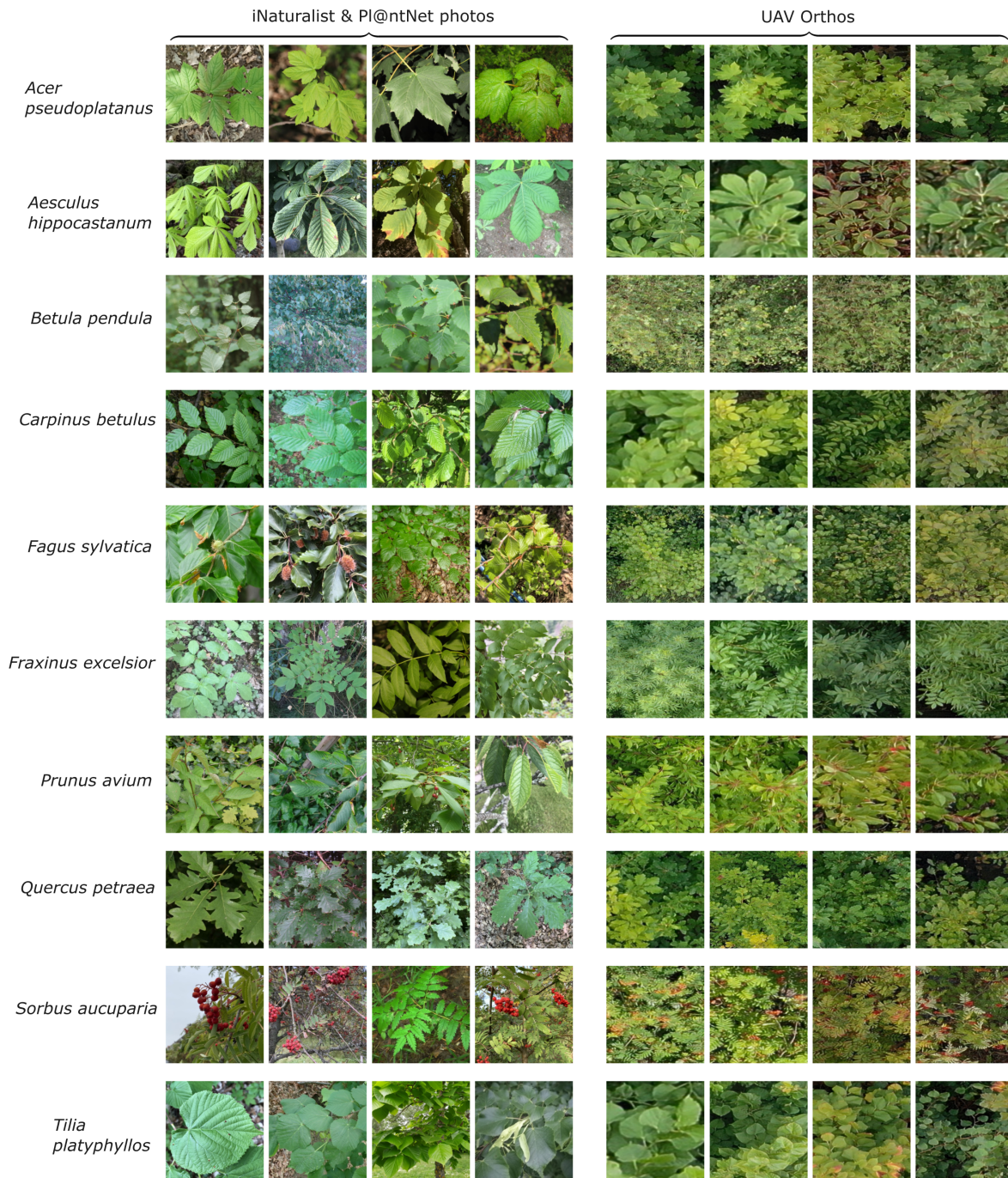


Figure 3: Example citizen science-based photographs derived from iNaturalist and tiles of UAV orthoimages (512 * 512 pixels) for the ten tree species in the MyDiv experiment.

190 The acquisition settings of citizen science plant photographs are heterogeneous and differ
 191 considerably from the typical bird perspective of UAV orthoimages (Fig. 3). For instance, from
 192 the UAV perspective, canopies are mostly viewed from a relatively homogeneous distance, and
 193 the photographs represent mostly leaves and other crown components. In contrast, the citi-
 194 zen science data includes a lot of close-ups, landscape imagery, or horizontal photographs of

195 trunks. [Soltani et al. \(2022\)](#) has demonstrated that species recognition in UAV images can be
196 improved by excluding crowd-sourced photographs that are exceptionally close (e.g., showing
197 individual leaf veins) or too far away from the plant (e.g., landscape images). Therefore,
198 we filtered the citizen science-based training photos according to the camera-plant-distance.
199 Moreover, we filtered photos that exclusively contained tree stems. Because such information
200 is unavailable in the citizen science datasets, we trained CNN-based regression and classifi-
201 cation models to predict acquisition distance and tree trunk presence for each downloaded
202 photograph. To train these CNN-based models, we visually estimated the acquisition distance
203 (4,500 photographs) and labeled tree trunk presence (1,000 photographs). To ease the label-
204 ing process, we used previously labeled training data from ([Soltani et al., 2022](#)) and added
205 150 additional tree photographs from the tree species present in the MyDiv experimental site.

206 To evaluate the models for predicting the acquisition distance and trunk presence, We
207 randomly split the citizen science-based plant photographs into training and validation sets,
208 with 80% for training and 20% for validation.

209 For the distance regression and the trunk classification, we used the EfficientNetB7 back-
210 bone ([Tan and Le, 2019](#)). For the distance regression, we used the following top-layer settings:
211 global average pooling, batch normalization, drop out (rate 0.1), and a final dense layer with
212 1 unit and linear activation function. We used the Adam optimizer (learning rate of 0.0001)
213 and a mean squared error (MSE) loss function. For the trunk classification, we used the
214 following top-layer settings: global max-pooling, a final dense layer with two units, and a
215 softmax activation function. We used the Adam optimizer (learning rate of 0.0001) and the
216 categorical cross-entropy loss function. Both models were trained using a batch size of 20 and
217 50 epochs.

218 We used the model with the lowest loss from these epochs (details on the model perfor-
219 mance are given in [Appendix A1.3](#)) to predict the acquisition distance and tree trunk presence
220 in all downloaded photographs for our target species. We filtered training photographs prior
221 to training CNN-based species classification (see [section 2.2](#)) with acquisition distances less
222 than 0.2 m and greater than 15 m and photographs classified as trunk (probability threshold
223 of 0.5). Thereby, 82,628 of the 101,574 downloaded citizen science photographs remained.

224 **2.2 CNN-based creation of plant species segmentation masks using a mov-** 225 **ing window approach**

226 The segmentation masks were obtained using a CNN image classification model trained on
227 crowd-sourced plant photographs and simple species labels using a moving window method
228 (hereafter $\text{CNN}_{\text{window}}$, [Fig. 1](#))b. Based on the results of previous studies, we choose a generic
229 image size of 512×512 pixels for the CNN classification model ([Schiefer et al., 2020](#); [Soltani](#)
230 [et al., 2022](#)). During the moving window approach, the orthoimage is sequentially cropped into
231 tiles of 512×512 pixels on which the image classification is applied to predict the species for
232 each location. This procedure is applied with a dense overlap between tiles defined by a step
233 size, resulting in a dense regular grid of species predictions. We chose a vertical and horizontal
234 distance of 51 pixels as the step size. The resulting predictions were afterwards rasterized to

235 a continuous species distribution grid with a spatial resolution of 8.31 cm/pixel (see [Soltani](#)
236 [et al., 2022](#), for details). The $\text{CNN}_{\text{window}}$ model was implemented as a classification task with
237 eleven classes, including the ten tree species and the background class.

238 The number of available photographs varied widely across tree species (see [2.1.2](#)), poten-
239 tially biasing the model towards classes with more photographs. To address this imbalance,
240 we equally sampled 4,000 photographs for each class with replacements. Sampling with re-
241 placement randomly duplicates the existing photographs for under-represented classes, in this
242 case, classes with fewer than 4,000 photographs. We applied a data augmentation to increase
243 the variance of the duplicated images. The augmentation consisted of random vertical and
244 horizontal flips, random brightness with a maximum delta of 10% (± 0.1), and contrast al-
245 teration within a range of 90% to 110% (0.9 to 1.1) of training photographs. We randomly
246 partitioned the training data into validation and training sets to ensure unbiased evaluation.
247 From the training set, we allocated a holdout of 20% for model selection, while the remaining
248 80% was used for model training. Subsequently, we assessed the accuracy of the selected
249 model using the validation set.

250 After testing different architectures as model backbones, including ResNet-50V2, Effi-
251 cientNetB07, and EfficientNetV2L, we selected EfficientNetV2L as it resulted in the highest
252 classification accuracies. The following layers were added on top of the EfficientNetV2L back-
253 bone: Dropout with a ratio of 0.5, average pooling, dropout with a ratio of 0.5, a dense layer
254 with 128 units, L2 kernel regularizer (0.001), a ReLu activation function, and a final dense
255 layer with a softmax activation function and 11 units (corresponding to the ten tree species
256 and the background class). We used Root Mean Squared Propagation (RMSprop) as the
257 optimizer with a learning rate of 0.0001 and categorical cross-entropy as a loss function. We
258 trained the configured model with a batch size of 15 over 150 epochs. The model with the
259 lowest loss (based on the 20% holdout) was selected as the final model. The latter was used
260 to predict the tree species (probabilities) in the UAV orthoimages using the above-mentioned
261 $\text{CNN}_{\text{window}}$ method (Fig. 1b). To filter uncertain predictions (predominantly in canopy gaps
262 or at crown shadows), we only considered a tree species as predicted above a threshold higher
263 than 0.6. Otherwise, it was assigned to NA (not available) which accounts for approximately
264 7.8% of the image. To smooth the predictions and remove noise, we applied a sieve opera-
265 tion on the output of the $\text{CNN}_{\text{window}}$ (threshold = 50, considering horizontal, vertical, and
266 diagonal neighbors, R-package *terra*, vers. 1.7).

267 **2.3 CNN-based plant species segmentation using an encoder-decoder ar-** 268 **chitecture**

269 As encoder-decoder segmentation architecture (onwards $\text{CNN}_{\text{segment}}$), we chose U-Net ([Ron-](#)
270 [neberger et al., 2015](#)), which is the most widely applied segmentation method in remote
271 sensing image segmentation ([Kattenborn et al., 2021](#)). The U-Net architecture is a CNN-
272 based algorithm that performs semantic segmentation by predicting a class for each pixel of
273 the input image. The architecture consists of an encoder-decoder structure with skip connec-
274 tions. The configured architecture has four levels of convolutional blocks. Each convolutional

275 block consists of two convolutional layers and is followed by batch normalization and ReLU
276 activation. The encoder gradually compresses feature maps and reduces their spatial dimen-
277 sions via max pooling operations, while the decoder increases the feature map resolution by
278 transposed convolution. The encoder and decoder blocks are connected through skip connec-
279 tions, which transfer the spatial context of the encoder feature maps to the decoder, enabling
280 a segmentation at resolution of the input imagery in the last layer. The final layer has eleven
281 units (corresponding to the ten tree species and a background class). A corresponding softmax
282 activation function maps the features to class probabilities. Using a max function, the pixels
283 of the segmentation output are assigned to the class with the highest probability (Fig. A12).

284 The segmentation masks for training $\text{CNN}_{\text{segment}}$ were obtained from the predictions of the
285 $\text{CNN}_{\text{window}}$ method applied on both UAV orthoimages (section 2.2, Ortho_{July}, Ortho_{September}).
286 At first, we resampled the $\text{CNN}_{\text{window}}$ prediction maps to the original spatial resolution of the
287 orthoimages (0.22 cm pixel size). Afterward, we cropped the orthoimages and the prediction
288 maps into non-overlapping tiles, each with a size of 512×512 pixels, resulting in a total of
289 44,980 and 37,113 tiles from Ortho_{July} and Ortho_{September}, respectively.

290 The training data obtained from the $\text{CNN}_{\text{window}}$ approach were filtered to avoid training
291 the $\text{CNN}_{\text{segment}}$ model with uncertain predictions. Thereby, we assumed that predictions
292 for a tile are uncertain when the model predicts multiple classes with low relative cover.
293 Thus, after initial tests, we included only those tiles where the cover of at least one class
294 exceeded 30%. The number of training tiles per class after filtering varied between 1257 and
295 16894 samples; *Acer pseudoplatanus* (6581), *Aesculus hippocastanum* (2054), *Betula pendula*
296 (4955), *Carpinus betulus* (1535), *Fagus sylvatica* (16894), *Fraxinus excelsior* (7901), *Prunus*
297 *avium* (1257), *Quercus petraea* (1302), *Sorbus aucuparia* (5473), *Tilia platyphyllos* (1982),
298 Background (5408).

299 Similar to the previous $\text{CNN}_{\text{window}}$ classification task, the availability of training tiles
300 varied greatly across the tree species. This class imbalance may have partially stemmed from
301 the more systematic misclassification of certain classes during the $\text{CNN}_{\text{window}}$ prediction. To
302 reduce the unfavorable effects of a class imbalance on model training, we sampled 4,000 tiles
303 per class with replacement (similar to the $\text{CNN}_{\text{window}}$ procedure). We applied the same data
304 augmentation strategy as for the $\text{CNN}_{\text{window}}$ workflow to increase variance among duplicates.
305 20% of the training data were withheld for model selection.

306 We trained the U-Net architecture ($\text{CNN}_{\text{segment}}$) using Root Mean Squared Propagation
307 (RMSprop) as the optimizer with a learning rate of 0.0001 and an adapted Dice loss function.
308 We adapted the Dice loss to ignore the weights coming from pixels with NA mask values. The
309 models were trained with a batch size of 20 over 150 epochs.

310 The $\text{CNN}_{\text{segment}}$ was then applied to Ortho_{July} and Ortho_{September}. To reduce uncertain
311 predictions of $\text{CNN}_{\text{segment}}$, we assigned the pixels where predicted probabilities for any of
312 the tree species did not exceed 30 % to the background class. Thereby, we assumed that
313 uncertain predictions predominantly occur in canopy gaps. As image segmentation typically
314 suffers from increased uncertainty at tile edges, we repeated the predictions with horizontal
315 and vertical shifts of 256 pixels, which were subsequently aggregated using a majority vote.

316 The final model performance of $\text{CNN}_{\text{segment}}$ was assessed and compared to $\text{CNN}_{\text{window}}$
317 using the independent reference data (transects) obtained from the visual interpretation of
318 the UAV orthoimages.

319 **3 Results**

320 For the $\text{CNN}_{\text{window}}$ method, F1-scores differed considerably across the tree species, although
321 these differences were relatively consistent across the two orthoimages, i.e. $\text{Ortho}_{\text{July}}$ and
322 $\text{Ortho}_{\text{September}}$ (Fig. 4a, b). On a plot level, comparably high model performance (mean F1 >
323 0.6) was found for *Acer pseudoplatanus* and *Fraxinus excelsior*, followed by the intermediate
324 performance (mean F1-score 0.35-0.55) for *Aesculus hippocastanum*, *Sorbus aucuparia*, *Tilia*
325 *platyphyllos*, *Betula pendula*, and *Carpinus betulus*. Low performance (mean F1-score < 0.35)
326 was found for *Quercus petraea*, *Fagus sylvatica*, and *Prunus avium*. Averaged across species,
327 there was a slight decrease in model performance from $\text{Ortho}_{\text{July}}$ with a mean F1-score of 0.44
328 to $\text{Ortho}_{\text{September}}$ with a mean F1-score of 0.4 (Fig. 4a, b). Note that $\text{Ortho}_{\text{July}}$ corresponded
329 to the peak of the season, where leaves and canopies were still fully developed.

330 The $\text{CNN}_{\text{segment}}$ model performance across species was similar but generally higher com-
331 pared to the $\text{CNN}_{\text{window}}$ method. For $\text{Ortho}_{\text{July}}$ F1-scores increased from 0.44 to 0.48 (Fig. 4a
332 vs. c) and for $\text{Ortho}_{\text{September}}$, F1-scores increased from 0.40 to 0.46 (Fig. 4b vs. d).

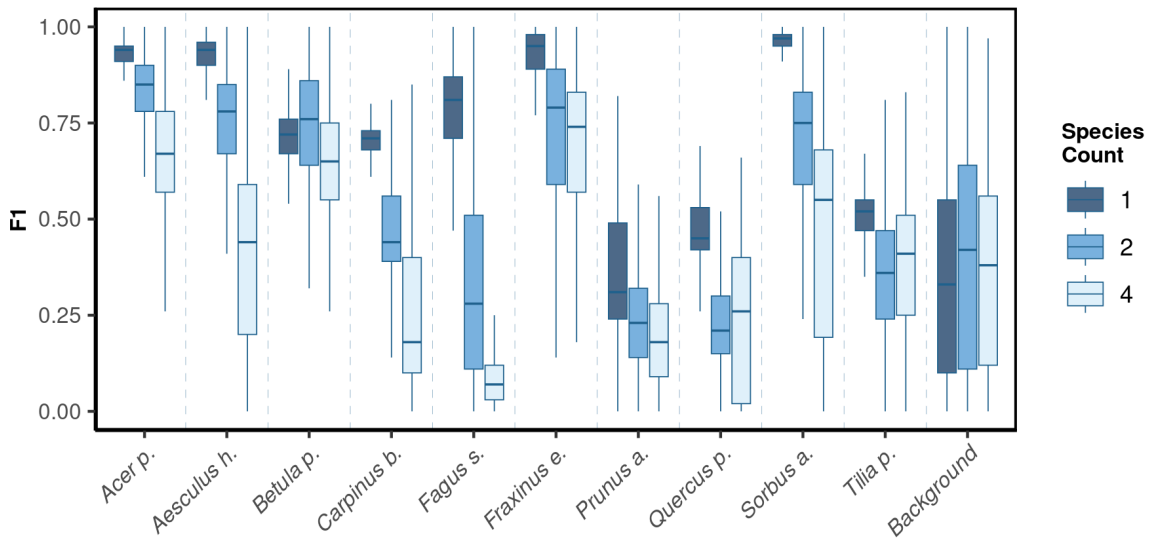
333 We observed notable differences in model performance (mean F1) across different species
334 mixtures, which are plots having one, two, or four species per plot (Fig. 5). For both
335 $\text{CNN}_{\text{window}}$ and $\text{CNN}_{\text{segment}}$, the model performance strongly increased with lower number
336 of species per plot (Fig. A13; results for $\text{CNN}_{\text{window}}$ are given in the Appendix).

337 The model performance of $\text{CNN}_{\text{segment}}$ exceeded the model performance of $\text{CNN}_{\text{window}}$
338, particularly in plots with an increased number of species: For monocultures, the relative
339 increase in model performance (F1-score) amounted to 2.5%, in two species plots to 6.9%,
340 and in plots with four species to 20.9% (averaged for $\text{Ortho}_{\text{July}}$ and $\text{Ortho}_{\text{September}}$). This
341 increased performance can be attributed to the advantages of the encoder-decoder principle
342 of the $\text{CNN}_{\text{segment}}$ method, enabling a pixel-wise and contextual prediction at the original
343 resolution of the orthomosaics. These advantages are also visible in Fig. 6, where $\text{CNN}_{\text{segment}}$
344 resulted in more detailed and accurate tree species segmentation (particularly for plots 26 and
345 29).

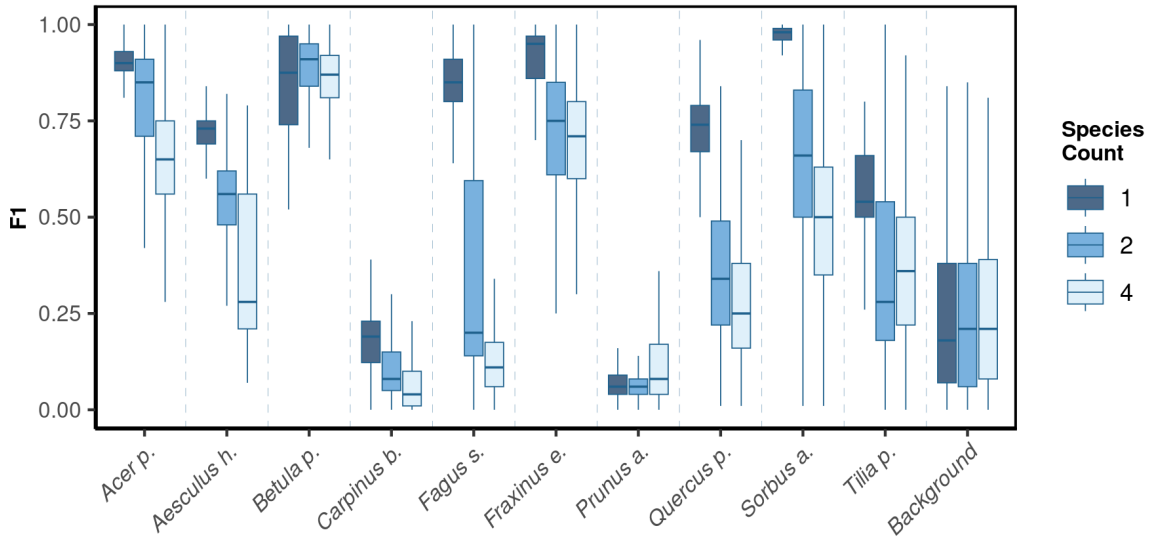
346 The highest model performance for $\text{CNN}_{\text{segment}}$ was found in monoculture plots, where F1-
347 scores > 0.5 were found for eight out of ten species for both $\text{Ortho}_{\text{July}}$ and $\text{Ortho}_{\text{September}}$. A
348 considerably lower performance for the July and September acquisition was found for *Prunus*
349 *avium*, which may correspond to similarities in leaf and canopy structure with *Fagus sylvatica*
350 and *Fraxinus excelsior* (a confusion matrix is given in the Appendix, Fig. A11). The decreased
351 performance for *Carpinus betulus* and *Prunus avium* in $\text{Ortho}_{\text{September}}$ can be attributed to
352 the very advanced senescence and leaf loss.

353 In addition to the increase in model performance, our analysis revealed that the prediction
354 on orthoimagery using $\text{CNN}_{\text{segment}}$ only required 10% of the computation time compared to

355 CNN_{window} . The duration of applying the models to the whole MyDiv orthomosaics covering
 356 an area of (3.02 hectares; 0.22 cm ground sampling distance) took approximately 27.05 hours
 357 with CNN_{segment} and 264.88 hours with CNN_{window} (NVIDIA A6000 with 48 GB RAM).

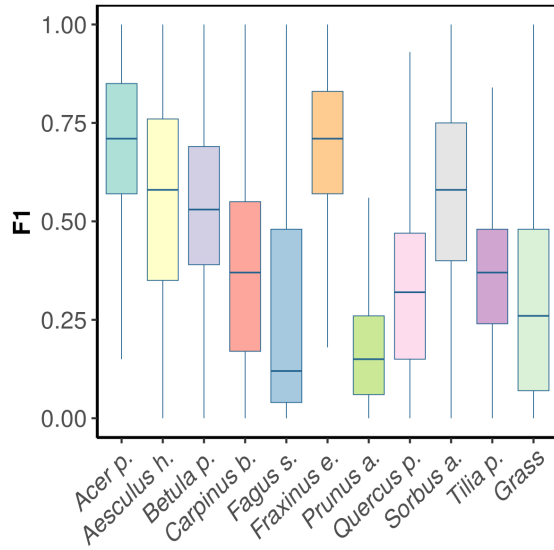


(a) Performance across species mixtures (F1-scores) on Ortho_{July}. Mean F1-scores: 1 species (0.51), 2 species (0.44), 4 species (0.41)

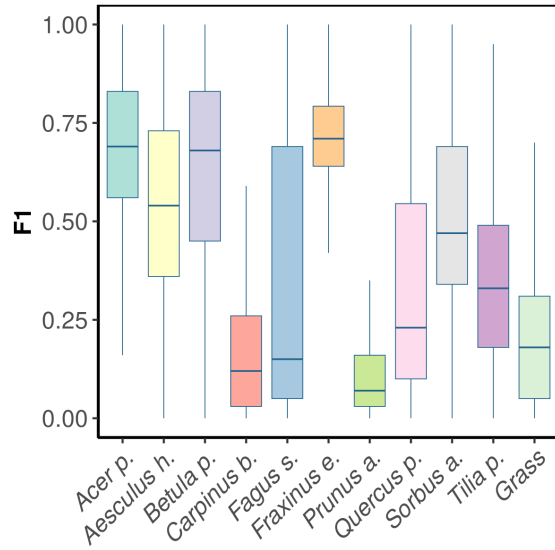


(b) Performance across species mixtures (F1-scores) on Ortho_{September}. Mean F1-scores: 1 species (0.58), 2 species (0.51), 4 species (0.42)

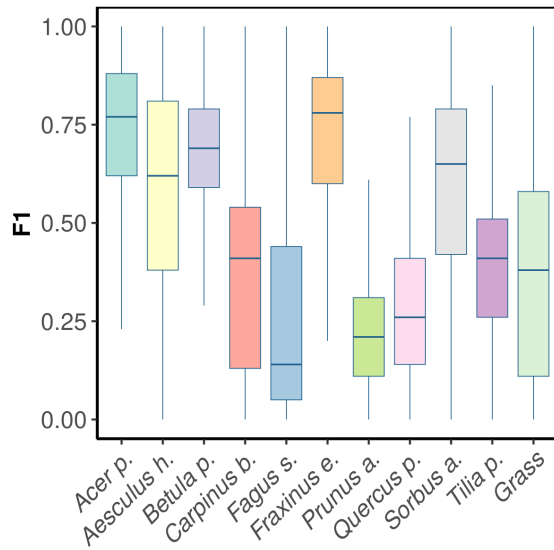
Figure 5: The model performance (F1-score) of the CNN_{segment} model across a gradient of canopy complexity in Ortho_{July} and Ortho_{September}. F1-scores decrease with increasing canopy complexity in plots



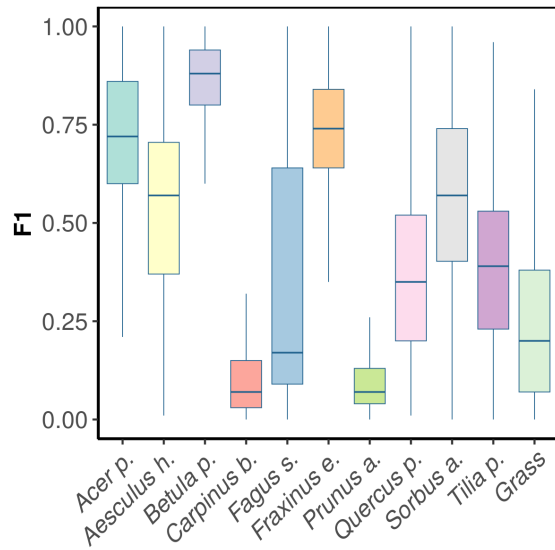
(a) F1-scores for $\text{CNN}_{\text{window}}$ on $\text{Ortho}_{\text{July}}$ (mean 0.44).



(b) F1-scores of $\text{CNN}_{\text{window}}$ on $\text{Ortho}_{\text{September}}$ (mean 0.42).



(c) F1-scores of $\text{CNN}_{\text{segment}}$ on $\text{Ortho}_{\text{July}}$ (mean 0.48).



(d) F1-scores of $\text{CNN}_{\text{segment}}$ on $\text{Ortho}_{\text{September}}$ (mean 0.46).

Figure 4: F1-scores by tree species and background class for $\text{Ortho}_{\text{July}}$ and $\text{Ortho}_{\text{September}}$ derived from $\text{CNN}_{\text{window}}$ and $\text{CNN}_{\text{segment}}$.

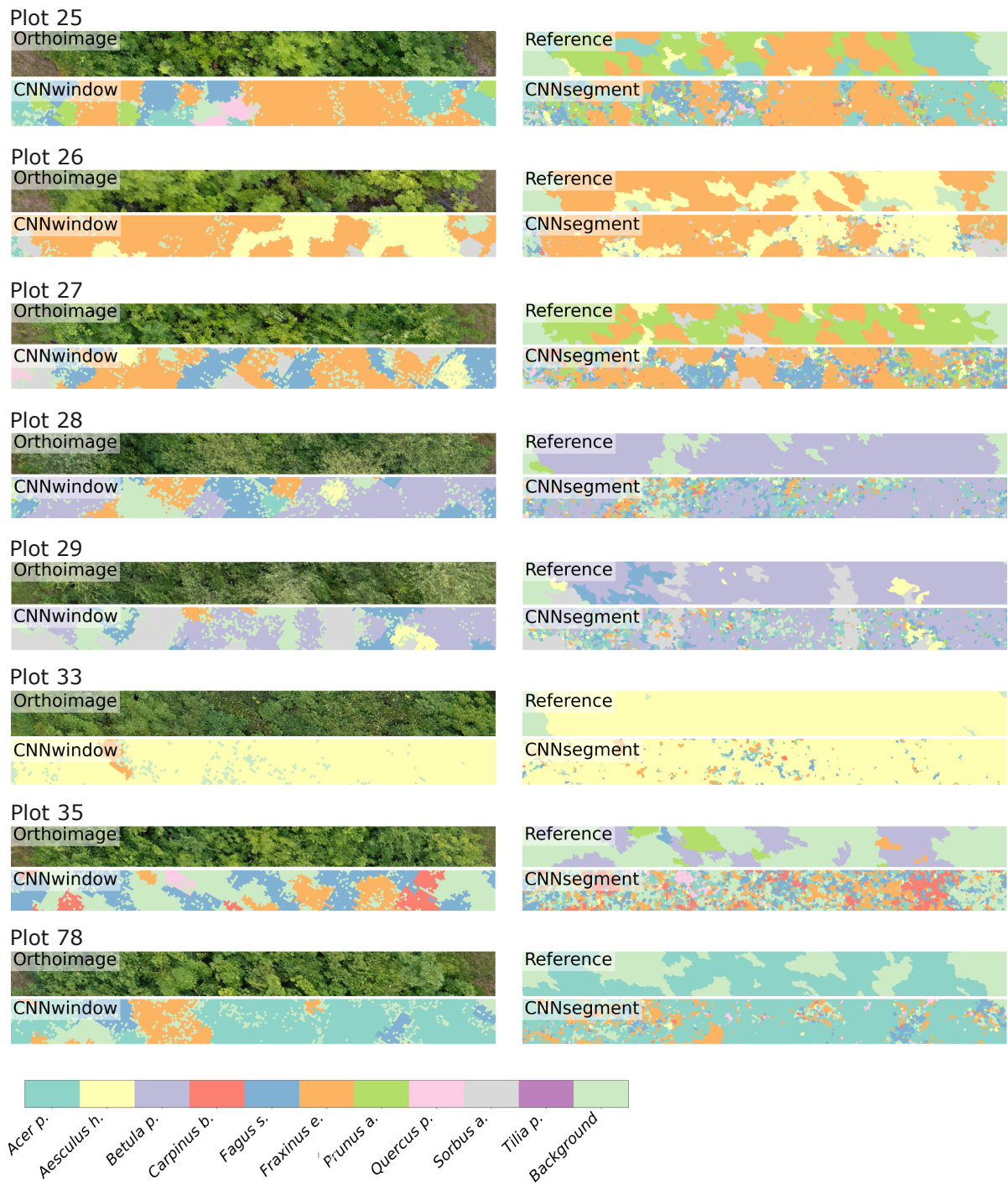


Figure 6: Transects of 2 m by 20 m of selected plots, including the orthoimage, the reference, CNN_{window} predictions, and $CNN_{segment}$ predictions. Visualizations for the remaining plots are given in the Appendix (Section A1.1).

358 4 Discussion

359 4.1 Filtering of citizen science data for drone-related applications

360 To achieve better correspondence between plant features visible in the citizen science pho-
361 tographs and the UAV images, we filtered the crowd-sourced photographs based on their
362 acquisition distance (less than 0.3 m or greater than 15 m) to exclude macro and landscape
363 photographs. Moreover, we excluded photographs that predominantly display tree stems,
364 facilitating a foliage-centric perspective as intrinsic to high-resolution UAV images (Fig. 3).
365 In the future, more criteria may be considered for filtering citizen science imagery, includ-
366 ing metadata (labels) on the presence of specific plant organs within an image (e.g., fruits,
367 flowers) as provided as a by-product by some citizen science plant identification apps (e.g.,
368 Pl@ntNet).

369 4.2 The creation of segmentation masks from simple image labels

370 One of the challenges of generating segmentation masks for the encoder-decoder method
371 ($\text{CNN}_{\text{segment}}$) with the proposed workflow may be error propagation between the different
372 steps. Firstly, the CNN image classification trained on the citizen science data has varying
373 uncertainty for the different species, resulting from noisy citizen science observations or lim-
374 itations to identify some species solely by photographs (Van Horn et al., 2018). Secondly,
375 the moving window approach ($\text{CNN}_{\text{window}}$), which predicts one species for an entire tile, may
376 be too coarse to resemble very complex canopies (e.g., in highly diverse plant communities).
377 However, although the fact that the segmentation labels created with the $\text{CNN}_{\text{window}}$ ap-
378 proach are partially inaccurate (Fig. 4a, 6), we found that the $\text{CNN}_{\text{segment}}$ procedure indeed
379 resulted in higher performance than the $\text{CNN}_{\text{window}}$ procedure. This is in line with other
380 studies (Kattenborn et al., 2021; Cloutier et al., 2023; Schiller et al., 2021) reporting that
381 deep learning-based pattern recognition can partially overcome noisy labels, whereas the in-
382 tentional use of noisy reference data, also known as weakly-supervised learning, is generally
383 very promising in the absence of high-quality labels (Cherif et al., 2023; Zhou, 2018; Schiller
384 et al., 2021). Here, we filtered the training data (masks) for regions where we expect extreme
385 noise levels, that is, for tiles where none of the classes exceeded a relative cover of 30%. These
386 regions were, according to our observation, often canopy gaps and shadowed areas, where one
387 naturally expects lower model performance as species-specific textures are less visible (Lopatin
388 et al., 2019; Milas et al., 2017; De Sa et al., 2018).

389 The enhanced segmentation performance of the $\text{CNN}_{\text{segment}}$ approach compared to $\text{CNN}_{\text{window}}$
390 can be attributed to the spatially explicit and finer-resolved predictions of the U-Net segmen-
391 tation algorithm (encoder-decoder principle), enabling a segmentation of the tree species at
392 the native resolution of the orthoimagery. The $\text{CNN}_{\text{segment}}$ approach resulted in improved
393 prediction results compared to the $\text{CNN}_{\text{window}}$ method in plots with more species and, hence,
394 more complex canopies. Thus, the presented two-step approach of creating segmentation
395 masks from simple class labels $\text{CNN}_{\text{window}}$, as provided by iNaturalist and Pl@ntNet plat-
396 forms, can indeed be used to create segmentation masks required for state-of-the-art image

397 analysis methods ($\text{CNN}_{\text{segment}}$) and thereby result in high value for remote sensing applica-
398 tions. The increased value of these segmentation masks enables the training of algorithms
399 with higher performance in species recognition. It greatly enhances the computational effi-
400 ciency of applying the models on orthoimagery (approximately ten times faster). Especially
401 for recurrent applications, such as monitoring or large-scale undertakings, the two-step ap-
402 proach involving the creation of segmentation masks and encoder-decoder architectures is
403 recommended.

404 **4.3 The role of canopy complexity**

405 Overall, the segmentation performance declined with increasing species richness per plot.
406 We expect that this can mainly be attributed to the small size of individual trees at the
407 MyDiv site, where in high species mixtures, there is a lower chance that a 512×512 pixel
408 tile includes clearly visible species-specific leaf and branching patterns. This also explains
409 why, in particular, trees with lower relative canopy height (e.g., *Quercus petrea* and *Fagus*
410 *sylvatica*) were less likely to be accurately segmented in species mixtures. The observed effect
411 of canopy complexity is in line with previous findings from [Soltani et al. \(2022\)](#); [Lopatin](#)
412 [et al. \(2017\)](#); [Fassnacht et al. \(2016\)](#); [Fricker et al. \(2019\)](#), where smaller patches of individual
413 species were less likely to be accurately detected. Visual inspection also confirmed that
414 false predictions were more likely at canopy edges between different tree species (Fig. 6).
415 However, it should be noted that the small-scaled canopy complexity of the plots used here
416 is exceptionally high (Fig. 3). Most tree crowns in the MyDiv experiment do not exceed a
417 diameter of 1.5 m, and the transition among tree crowns of multiple species is often very
418 fuzzy. Thus, we expect reduced performance in canopy transitions to be less relevant in
419 real-world settings, where tree species appear in more extensive, homogeneous patches and
420 where individual crowns are commonly larger. Thus, the model performance in these species
421 mixtures can be interpreted as a rather conservative estimate. The results obtained for the
422 monocultures might be more representative in terms of real-world applications, as mature
423 trees in temperate forests typically have crown diameters 5 to 20 times larger. Application
424 tests of the presented approach in real forests are desirable. However, acquiring such a dataset
425 is a logistical challenge since temperate forest stands commonly do not feature a comparably
426 high and balanced occurrence of that many tree species.

427 **4.4 Spatial resolution of the UAV imagery is key**

428 According to the results obtained in the monocultures, The $\text{CNN}_{\text{segment}}$ model successfully
429 classified seven out of ten tree species ($F1 > 0.7$). The lower F1-scores for *Quercus petrea*
430 (mean F1 0.57), *Prunus avium*(mean F1 0.2), *Tilia platyphyllos*(mean F1 0.53) may result
431 from the spectral and morphological similarity at the current spatial resolution of the UAV
432 imagery (0.22 cm)(Fig. 3). Hence, there was a tendency that these species were often confused
433 with each other (see confusion matrices in Appendix A1.2). Such confusion among plants
434 with a similar appearance was confirmed by other studies ([Cloutier et al., 2023](#); [Schiefer](#)

435 [et al., 2020](#), e.g.) and matches our experience from the generation of reference data via visual
436 interpretation, where a separation between these species was sometimes challenging. Initial
437 CNN-based segmentation attempts (results not shown) in the preparation of this study were
438 based on an orthoimage of 0.3 cm instead of 0.22 cm resolution, resulting in clearly lower
439 model performances. This aligns with the reported importance of spatial resolution of UAV
440 imagery for CNN segmentation of earlier studies ([Schiefer et al., 2020](#); [Schmitt et al., 2020](#);
441 [Ma et al., 2019](#); [G. Braga et al., 2020](#)). Thus, while the current orthoimages with 0.22 cm
442 resolution delivered promising results, further increasing the spatial resolution might be very
443 promising for species where characteristic leaf forms are only visible at fine spatial resolutions.

444 **4.5 Model transferability across seasons and orthoimage acquisition prop-** 445 **erties**

446 The variability of human behavior and electronic devices makes citizen science-based plant
447 photographs very heterogeneous. This can be a challenge for deep learning applications, such
448 as species recognition or plant trait characterization ([Schiller et al., 2021](#); [Van Horn et al.,](#)
449 [2021](#); [van Der Velde et al., 2023](#); [Affouard et al., 2017](#)), where models have to identify features
450 that hold across various viewing angles, distances, or illumination conditions. However, this
451 heterogeneity might also be of great value, given that citizens depict the appearance of plants
452 under various site, environmental, and phenological conditions. This, in turn, offers a unique
453 setting for training models that are generic and transferable across these conditions. Here, we
454 evaluated the transferability of our models across different data sets by applying them to two
455 orthoimages acquired in different seasons (peak of growing season and autumn). Both the
456 $\text{CNN}_{\text{window}}$ and $\text{CNN}_{\text{segment}}$ models could identify deciduous tree species in the orthoimages
457 with surprising accuracies, suggesting that the models are transferable to different conditions.

458 **4.6 Outlook**

459 Overall, our results indeed highlight the value of citizen science photographs with simple class
460 labels to create training data for state-of-the-art segmentation approaches. A great advan-
461 tage of this citizen science-based approach is that it does not require often costly training
462 data obtained from visual interpretation or field surveys (here, reference data was only used
463 for validating the models). This particularly highlights the potential of citizen science data
464 for applications where many species are of interest, such as biodiversity-related monitoring
465 applications ([Chandler et al., 2017](#); [Johnston et al., 2023](#)). In this regard, data or models of
466 species-recognition platforms that incorporate excessive amounts of plant species and respec-
467 tive imagery are very promising, including iNaturalist ([Boone and Basille, 2019](#)), Pl@ntNet
468 ([Affouard et al., 2017](#)), ObsIdentify ([Molls, 2021](#)) or FloraIncognita ([Mäder et al., 2021](#)). Yet,
469 based on the current and the precursor study ([Soltani et al., 2022](#)), we expect that a pre-
470 selection of citizen science photograph databases considering images more representative of
471 the common UAV-based perspective is required to unleash the potential of this heterogeneous
472 data.

473 5 Conclusion

474 The transfer learning approach presented here demonstrates the value of freely available
475 crowd-sourced plant photographs for remote sensing studies. This heterogeneous dataset
476 can provide valuable training data for transferable CNN-based segmentation models. Here,
477 this potential was highlighted in a very complex task, i.e., the differentiation of 10 temperate
478 deciduous tree species in mixed vegetation stands with a complex structure. The presented
479 two-step approach demonstrated how we can transfer and harness generic knowledge gathered
480 by citizens on how plants 'look' to the bird perspective of high-resolution drone imagery. The
481 presented moving window approach overcomes the limitation of citizen science-based pho-
482 tographs having only simple species labels. The segmentation maps derived from an image
483 classification model applied in a moving window setting can be harnessed to create segmen-
484 tation masks for encoder-decoder-type segmentation models. The latter does not only enable
485 higher accuracies in species segmentation but is also considerably more efficient. By building
486 on the effort of thousands of citizens, this framework enables the mapping of plant species
487 without any training data obtained from visual interpretation or ground-based field surveys.
488 Due to the large amounts of plant photographs acquired in different conditions, such models
489 can be assumed to have good transferability.

490 6 Data and code availability

491 The code used in this study is publicly accessible via our GitHub repository at [https://](https://github.com/salimsoltani28/CrowdVision2TreeSegment)
492 github.com/salimsoltani28/CrowdVision2TreeSegment. The data supporting the findings
493 of this research is available on Zonodo at <https://zenodo.org/uploads/10019552>.

494 7 Declaration of competing interest

495 The authors declare that they have no known competing financial interests or personal rela-
496 tionships that could have appeared to influence the work reported in this paper.

497 8 Acknowledgements

498 SS and TK acknowledge funding by the German Research Foundation (DFG) under the
499 project BigPlantSens (Assessing the Synergies of Big Data and Deep Learning for the Re-
500 mote Sensing of Plant Species; Project number 444524904) and PANOPS (Revealing Earth's
501 plant functional diversity with citizen science; project number 504978936). SS and HF ac-
502 knowledge financial support by the Federal Ministry of Education and Research of Germany
503 (BMBF) and by the Saechsische Staatsministerium für Wissenschaft, Kultur und Tourismus
504 in the program Center of Excellence for AI-research "Center for Scalable Data Analytics and
505 Artificial Intelligence Dresden/Leipzig", project identification number: ScaDS.AI. NE and OF
506 acknowledge funding by the Deutsche Forschungsgemeinschaft DFG (German Centre for In-

507 tegrative Biodiversity Research, FZT118; and Gottfried Wilhelm Leibniz Prize, Ei 862/29-1).
508 Moreover, we acknowledge support from University of Freiburg for Open Access Publishing.

509 References

- 510 A. Affouard, H. Goëau, P. Bonnet, J.-C. Lombardo, and A. Joly. Pl@ ntnet app in the era of
511 deep learning. In *ICLR: International Conference on Learning Representations*, 2017.
- 512 E. Bayraktar, M. E. Basarkan, and N. Celebi. A low-cost uav framework towards ornamental
513 plant detection and counting in the wild. *ISPRS Journal of Photogrammetry and Remote*
514 *Sensing*, 167:1–11, 2020.
- 515 M. E. Boone and M. Basille. Using inaturalist to contribute your nature observations to
516 science. *EDIS*, 2019(4):5–5, 2019.
- 517 A. Bouguettaya, H. Zarzour, A. Kechida, and A. M. Taberkit. Deep learning techniques to
518 classify agricultural crops through uav imagery: A review. *Neural Computing and Applica-*
519 *tions*, 34(12):9511–9536, 2022.
- 520 M. Brandt, C. J. Tucker, A. Kariryaa, K. Rasmussen, C. Abel, J. Small, J. Chave, L. V.
521 Rasmussen, P. Hiernaux, A. A. Diouf, et al. An unexpectedly large count of trees in the
522 west african sahara and sahel. *Nature*, 587(7832):78–82, 2020.
- 523 P. G. Brodrick, A. B. Davies, and G. P. Asner. Uncovering ecological patterns with convolu-
524 tional neural networks. *Trends in ecology & evolution*, 34(8):734–745, 2019.
- 525 M. Chandler, L. See, K. Copas, A. M. Bonde, B. C. López, F. Danielsen, J. K. Legind,
526 S. Masinde, A. J. Miller-Rushing, G. Newman, et al. Contribution of citizen science towards
527 international biodiversity monitoring. *Biological conservation*, 213:280–294, 2017.
- 528 E. Cherif, H. Feilhauer, K. Berger, P. D. Dao, M. Ewald, T. B. Hank, Y. He, K. R. Kovach,
529 B. Lu, P. A. Townsend, et al. From spectra to plant functional traits: Transferable multi-
530 trait models from heterogeneous and sparse data. *Remote Sensing of Environment*, 292:
531 113580, 2023.
- 532 M. Cloutier, M. Germain, and E. Laliberté. Influence of temperate forest autumn leaf phenol-
533 ogy on segmentation of tree species from uav imagery using deep learning. *bioRxiv*, pages
534 2023–08, 2023.
- 535 D. J. Curnick, A. J. Davies, C. Duncan, R. Freeman, D. M. Jacoby, H. T. Shelley, C. Rossi,
536 O. R. Wearn, M. J. Williamson, and N. Pettorelli. Smallsats: a new technological frontier
537 in ecology and conservation? *Remote Sensing in Ecology and Conservation*, 2021.
- 538 N. C. De Sa, P. Castro, S. Carvalho, E. Marchante, F. A. López-Núñez, and H. Marchante.
539 Mapping the flowering of an invasive plant using unmanned aerial vehicles: is there potential
540 for biocontrol monitoring? *Frontiers in plant science*, 9:293, 2018.

- 541 G. J. Di Cecco, V. Barve, M. W. Belitz, B. J. Stucky, R. P. Guralnick, and A. H. Hurlbert.
542 Observing the observers: How participants contribute data to inaturalist and implications
543 for biodiversity science. *BioScience*, 71(11):1179–1188, 2021.
- 544 F. E. Fassnacht, H. Latifi, K. Stereńczak, A. Modzelewska, M. Lefsky, L. T. Waser, C. Straub,
545 and A. Ghosh. Review of studies on tree species classification from remotely sensed data.
546 *Remote Sensing of Environment*, 186:64–87, 2016.
- 547 O. Ferlian, S. Cesarz, D. Craven, J. Hines, K. E. Barry, H. Bruelheide, F. Buscot, S. Haider,
548 H. Heklau, S. Herrmann, et al. Mycorrhiza in tree diversity–ecosystem function relation-
549 ships: conceptual framework and experimental implementation. *Ecosphere*, 9(5):e02226,
550 2018.
- 551 D. Fraisl, G. Hager, B. Bedessem, M. Gold, P.-Y. Hsing, F. Danielsen, C. B. Hitchcock, J. M.
552 Hulbert, J. Piera, H. Spiers, et al. Citizen science in environmental and ecological sciences.
553 *Nature Reviews Methods Primers*, 2(1):64, 2022.
- 554 G. A. Fricker, J. D. Ventura, J. A. Wolf, M. P. North, F. W. Davis, and J. Franklin. A
555 convolutional neural network classifier identifies tree species in mixed-conifer forest from
556 hyperspectral imagery. *Remote Sensing*, 11(19):2326, 2019.
- 557 J. R. G. Braga, V. Peripato, R. Dalagnol, M. P. Ferreira, Y. Tarabalka, L. E. OC Aragão,
558 H. F. de Campos Velho, E. H. Shiguemori, and F. H. Wagner. Tree crown delineation
559 algorithm based on a convolutional neural network. *Remote Sensing*, 12(8):1288, 2020.
- 560 N. C. Galuszynski, R. Duker, A. J. Potts, and T. Kattenborn. Automated mapping of por-
561 tulacaria afra canopies for restoration monitoring with convolutional neural networks and
562 heterogeneous unmanned aerial vehicle imagery. *PeerJ*, 10:e14219, 2022.
- 563 GBIF. Gbif: the global biodiversity information facility, 2019.
- 564 T. Hoeser and C. Kuenzer. Object detection and image segmentation with deep learning on
565 earth observation data: A review-part i: Evolution and recent trends. *Remote Sensing*, 12
566 (10):1667, 2020.
- 567 N. Ivanova and M. Shashkov. The possibilities of gbif data use in ecological research. *Russian*
568 *Journal of Ecology*, 52:1–8, 2021.
- 569 A. Johnston, E. Matechou, and E. B. Dennis. Outstanding challenges and future directions
570 for biodiversity monitoring using citizen science data. *Methods in Ecology and Evolution*,
571 14(1):103–116, 2023.
- 572 A. Joly, P. Bonnet, H. Goëau, J. Barbe, S. Selmi, J. Champ, S. Dufour-Kowalski, A. Affouard,
573 J. Carré, J.-F. Molino, et al. A look inside the pl@ ntnet experience: The good, the bias
574 and the hope. *Multimedia Systems*, 22:751–766, 2016.

- 575 T. Kattenborn, J. Eichel, and F. E. Fassnacht. Convolutional neural networks enable effi-
576 cient, accurate and fine-grained segmentation of plant species and communities from high-
577 resolution uav imagery. *Scientific reports*, 9(1):1–9, 2019a.
- 578 T. Kattenborn, J. Lopatin, M. Förster, A. C. Braun, and F. E. Fassnacht. Uav data as
579 alternative to field sampling to map woody invasive species based on combined sentinel-1
580 and sentinel-2 data. *Remote sensing of environment*, 227:61–73, 2019b.
- 581 T. Kattenborn, J. Leitloff, F. Schiefer, and S. Hinz. Review on convolutional neural networks
582 (cnn) in vegetation remote sensing. *ISPRS Journal of Photogrammetry and Remote Sensing*,
583 173:24–49, 2021.
- 584 T. Kattenborn, F. Schiefer, J. Frey, H. Feilhauer, M. D. Mahecha, and C. F. Dormann.
585 Spatially autocorrelated training and validation samples inflate performance assessment
586 of convolutional neural networks. *ISPRS Open Journal of Photogrammetry and Remote*
587 *Sensing*, 5:100018, 2022.
- 588 P. J. Leitão, M. Schwieder, F. Pötzschner, J. R. Pinto, A. M. Teixeira, F. Pedroni, M. Sanchez,
589 C. Rogass, S. van der Linden, M. M. Bustamante, et al. From sample to pixel: multi-scale
590 remote sensing data for upscaling aboveground carbon data in heterogeneous landscapes.
591 *Ecosphere*, 9(8):e02298, 2018.
- 592 J. Lopatin, F. E. Fassnacht, T. Kattenborn, and S. Schmidlein. Mapping plant species in
593 mixed grassland communities using close range imaging spectroscopy. *Remote Sensing of*
594 *Environment*, 201:12–23, 2017.
- 595 J. Lopatin, K. Dolos, T. Kattenborn, and F. E. Fassnacht. How canopy shadow affects invasive
596 plant species classification in high spatial resolution remote sensing. *Remote Sensing in*
597 *Ecology and Conservation*, 5(4):302–317, 2019.
- 598 L. Ma, Y. Liu, X. Zhang, Y. Ye, G. Yin, and B. A. Johnson. Deep learning in remote sensing
599 applications: A meta-analysis and review. *ISPRS journal of photogrammetry and remote*
600 *sensing*, 152:166–177, 2019.
- 601 P. Mäder, D. Boho, M. Rzanny, M. Seeland, H. C. Wittich, A. Deggelmann, and J. Wäldchen.
602 The flora incognita app—interactive plant species identification. *Methods in Ecology and*
603 *Evolution*, 2021.
- 604 W. H. Maes and K. Steppe. Perspectives for remote sensing with unmanned aerial vehicles
605 in precision agriculture. *Trends in plant science*, 24(2):152–164, 2019.
- 606 A. S. Milas, K. Arend, C. Mayer, M. A. Simonson, and S. Mackey. Different colours of
607 shadows: Classification of uav images. *International Journal of Remote Sensing*, 38(8-10):
608 3084–3100, 2017.

- 609 C. Molls. The obs-services and their potentials for biodiversity data assessments with a test
610 of the current reliability of photo-identification of coleoptera in the field. *Tijdschrift voor*
611 *Entomologie*, 164(1-3):143–153, 2021.
- 612 J. Müllerová, G. Brundu, A. Große-Stoltenberg, T. Kattenborn, and D. M. Richardson. Pat-
613 tern to process, research to practice: remote sensing of plant invasions. *Biological Invasions*,
614 pages 1–26, 2023.
- 615 O. Ronneberger, P. Fischer, and T. Brox. U-net: Convolutional networks for biomedical image
616 segmentation. In *International Conference on Medical image computing and computer-*
617 *assisted intervention*, pages 234–241. Springer, 2015.
- 618 M. Rzanny, P. Mäder, A. Deggelmann, M. Chen, and J. Wäldchen. Flowers, leaves or both?
619 how to obtain suitable images for automated plant identification. *Plant Methods*, 15(1):
620 1–11, 2019.
- 621 F. Schiefer, T. Kattenborn, A. Frick, J. Frey, P. Schall, B. Koch, and S. Schmidtlein. Mapping
622 forest tree species in high resolution uav-based rgb-imagery by means of convolutional neural
623 networks. *ISPRS Journal of Photogrammetry and Remote Sensing*, 170:205–215, 2020.
- 624 F. Schiefer, S. Schmidtlein, A. Frick, J. Frey, R. Klinke, K. Zielewska-Büttner, S. Junttila,
625 A. Uhl, and T. Kattenborn. Uav-based reference data for the prediction of fractional cover
626 of standing deadwood from sentinel time series. *ISPRS Open Journal of Photogrammetry*
627 *and Remote Sensing*, 8:100034, 2023.
- 628 C. Schiller, S. Schmidtlein, C. Boonman, A. Moreno-Martínez, and T. Kattenborn. Deep
629 learning and citizen science enable automated plant trait predictions from photographs.
630 *Scientific Reports*, 11(1):1–12, 2021.
- 631 M. Schmitt, J. Prexl, P. Ebel, L. Liebel, and X. X. Zhu. Weakly supervised semantic seg-
632 mentation of satellite images for land cover mapping—challenges and opportunities. *arXiv*
633 *preprint arXiv:2002.08254*, 2020.
- 634 S. Soltani, H. Feilhauer, R. Duker, and T. Kattenborn. Transfer learning from citizen science
635 photographs enables plant species identification in uavs imagery. *ISPRS Open Journal of*
636 *Photogrammetry and Remote Sensing*, page 100016, 2022.
- 637 Z. Sun, X. Wang, Z. Wang, L. Yang, Y. Xie, and Y. Huang. Uavs as remote sensing platforms
638 in plant ecology: review of applications and challenges. *Journal of Plant Ecology*, 14(6):
639 1003–1023, 2021.
- 640 M. Tan and Q. Le. Efficientnet: Rethinking model scaling for convolutional neural networks.
641 In *International conference on machine learning*, pages 6105–6114. PMLR, 2019.
- 642 M. van Der Velde, H. Goëau, P. Bonnet, R. d’Andrimont, M. Yordanov, A. Affouard,
643 M. Claverie, B. Czúcz, N. Elvekjær, L. Martinez-Sanchez, et al. Pl@ ntnet crops: merg-

- 644 ing citizen science observations and structured survey data to improve crop recognition for
645 agri-food-environment applications. *Environmental Research Letters*, 18(2):025005, 2023.
- 646 G. Van Horn, O. Mac Aodha, Y. Song, Y. Cui, C. Sun, A. Shepard, H. Adam, P. Perona, and
647 S. Belongie. The inaturalist species classification and detection dataset. In *Proceedings of*
648 *the IEEE conference on computer vision and pattern recognition*, pages 8769–8778, 2018.
- 649 G. Van Horn, E. Cole, S. Beery, K. Wilber, S. Belongie, and O. Mac Aodha. Benchmarking
650 representation learning for natural world image collections. In *Proceedings of the IEEE/CVF*
651 *Conference on Computer Vision and Pattern Recognition*, pages 12884–12893, 2021.
- 652 F. H. Wagner. The flowering of atlantic forest pleroma trees. *Scientific reports*, 11(1):1–20,
653 2021.
- 654 Z.-H. Zhou. A brief introduction to weakly supervised learning. *National science review*, 5
655 (1):44–53, 2018.

656 **A Appendix**

657 **A1.1 Prediction maps**

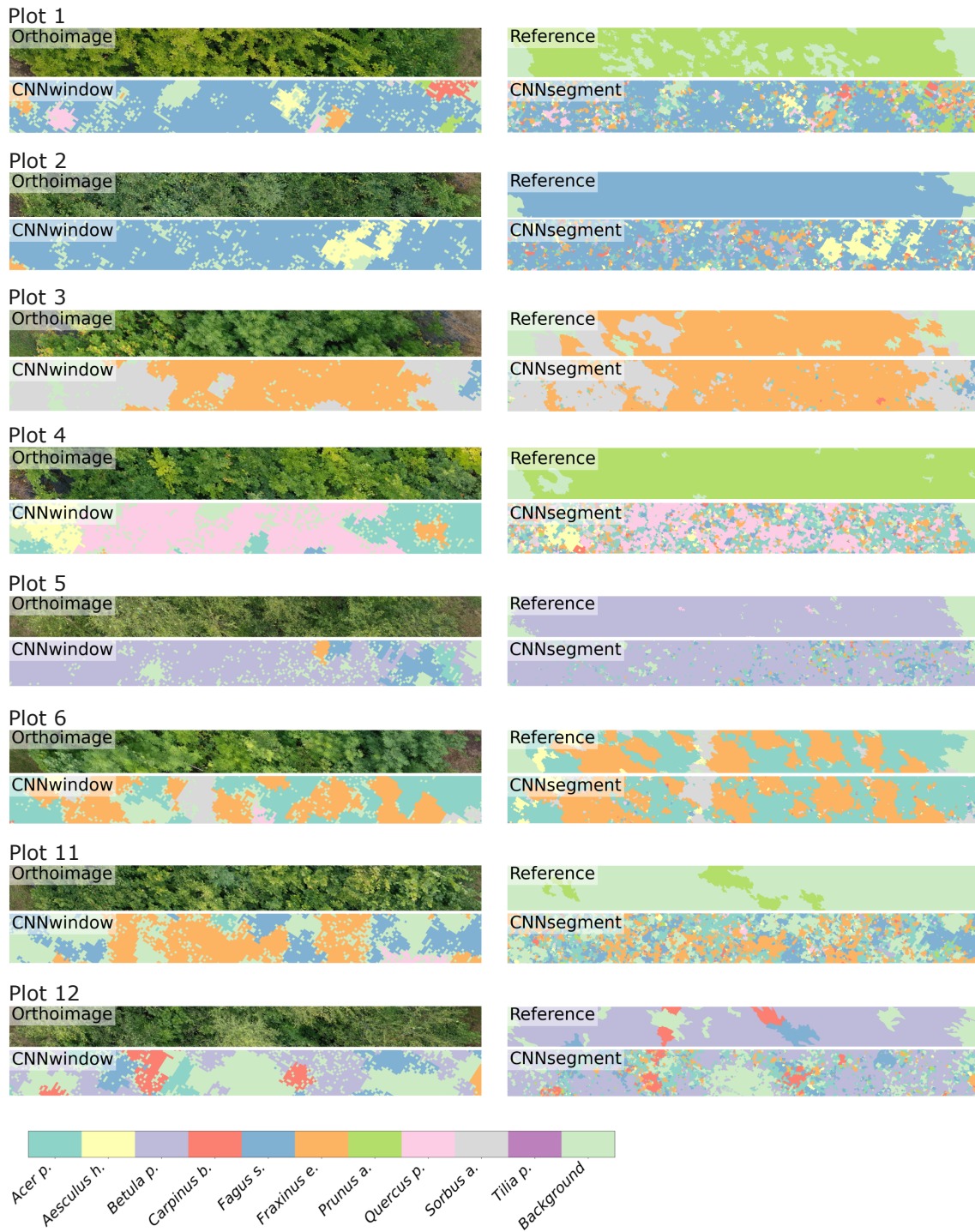


Figure A1: Transects of 2 m by 20 m of selected plots, including the orthoimage, the reference, CNN_{window} predictions, and $CNN_{segment}$ predictions.

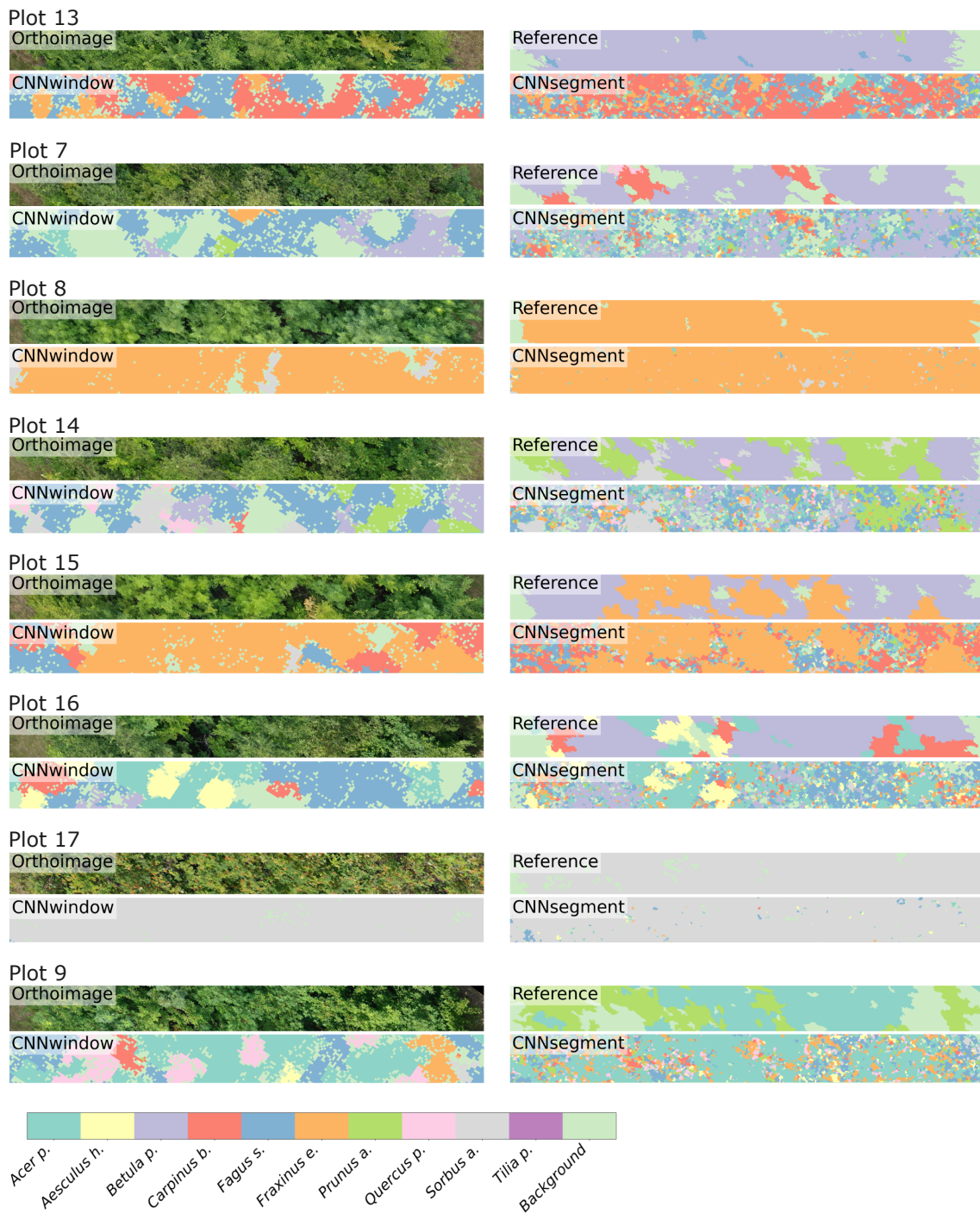


Figure A2: Transects of 2 m by 20 m of selected plots, including the orthoimage, the reference, CNN_{window} predictions, and CNN_{segment} predictions.

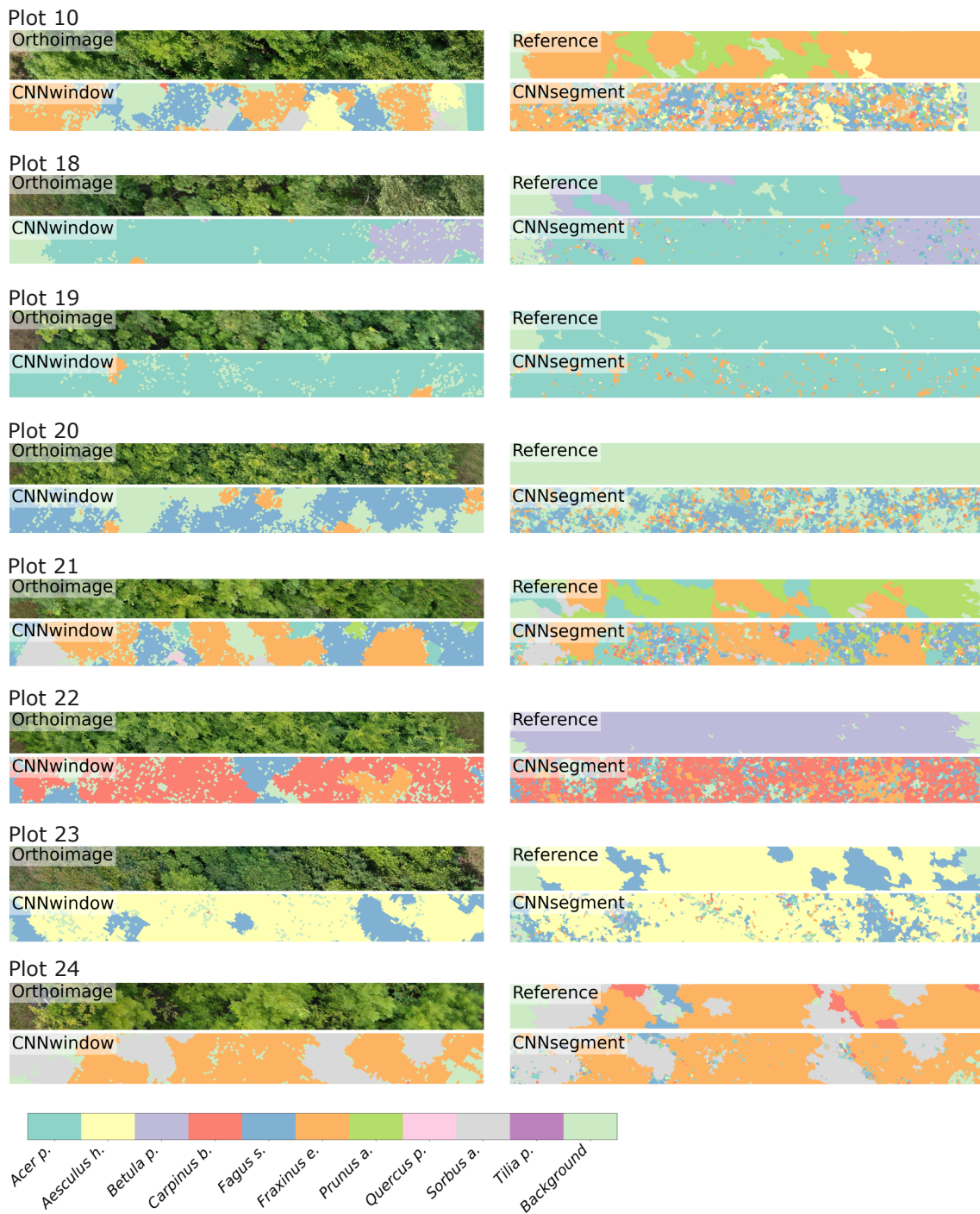


Figure A3: Transects of 2 m by 20 m of selected plots, including the orthoimage, the reference, CNN_{window} predictions, and CNN_{segment} predictions.

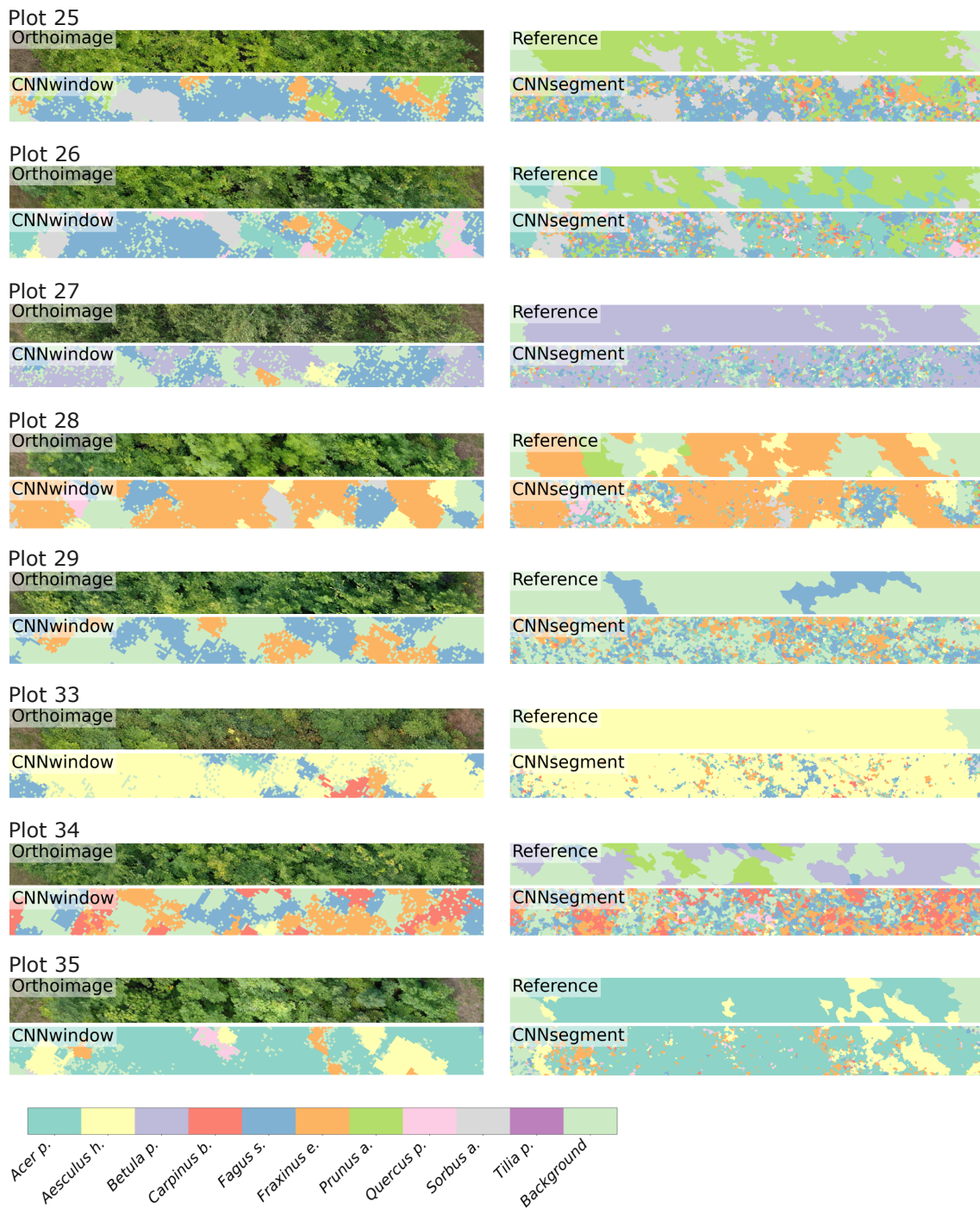


Figure A4: Transects of 2 m by 20 m of selected plots, including the orthoimage, the reference, CNN_{window} predictions, and CNN_{segment} predictions.

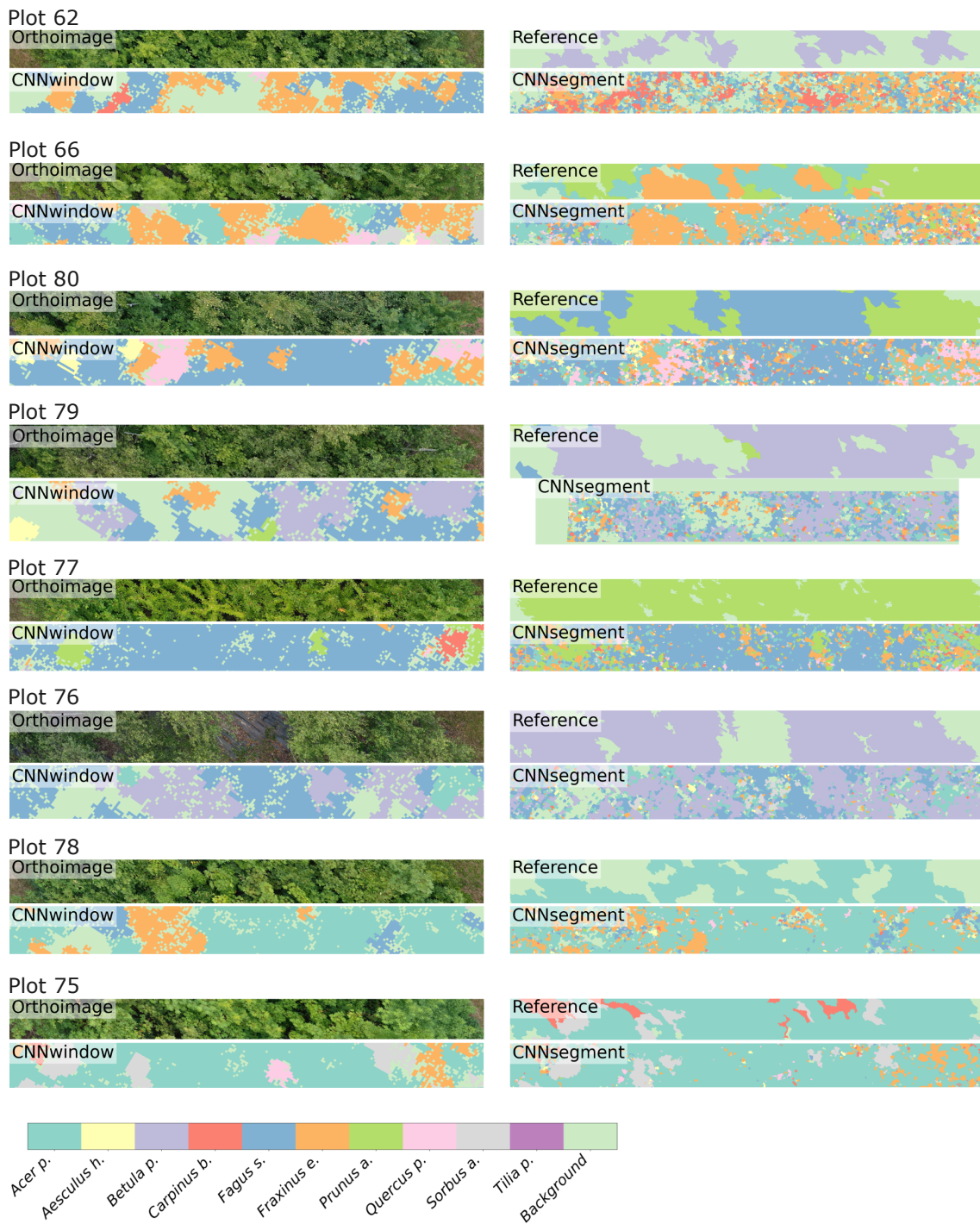


Figure A5: Transects of 2 m by 20 m of selected plots, including the orthoimage, the reference, CNN_{window} predictions, and CNN_{segment} predictions.

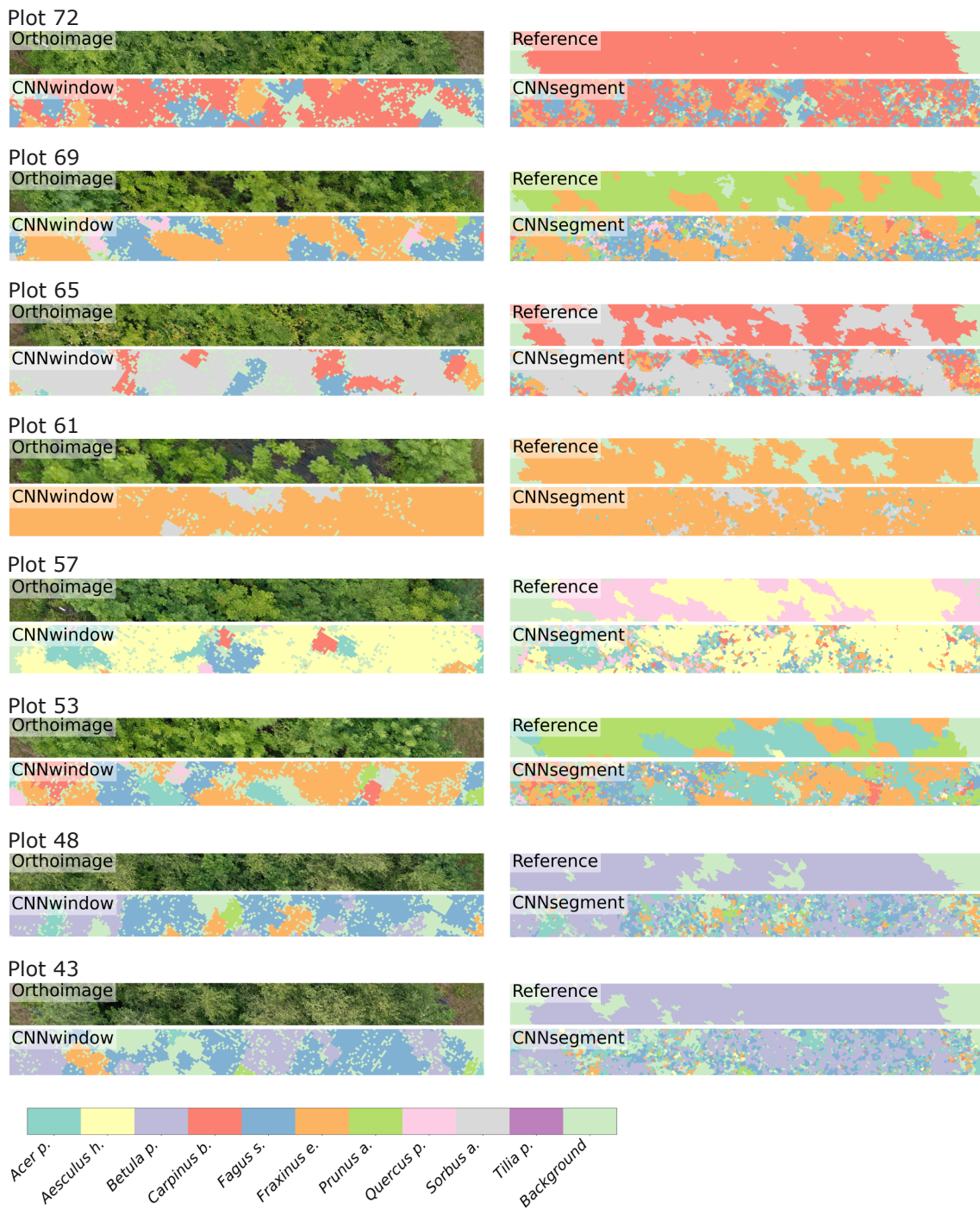


Figure A6: Transects of 2 m by 20 m of selected plots, including the orthoimage, the reference, CNN_{window} predictions, and CNN_{segment} predictions.

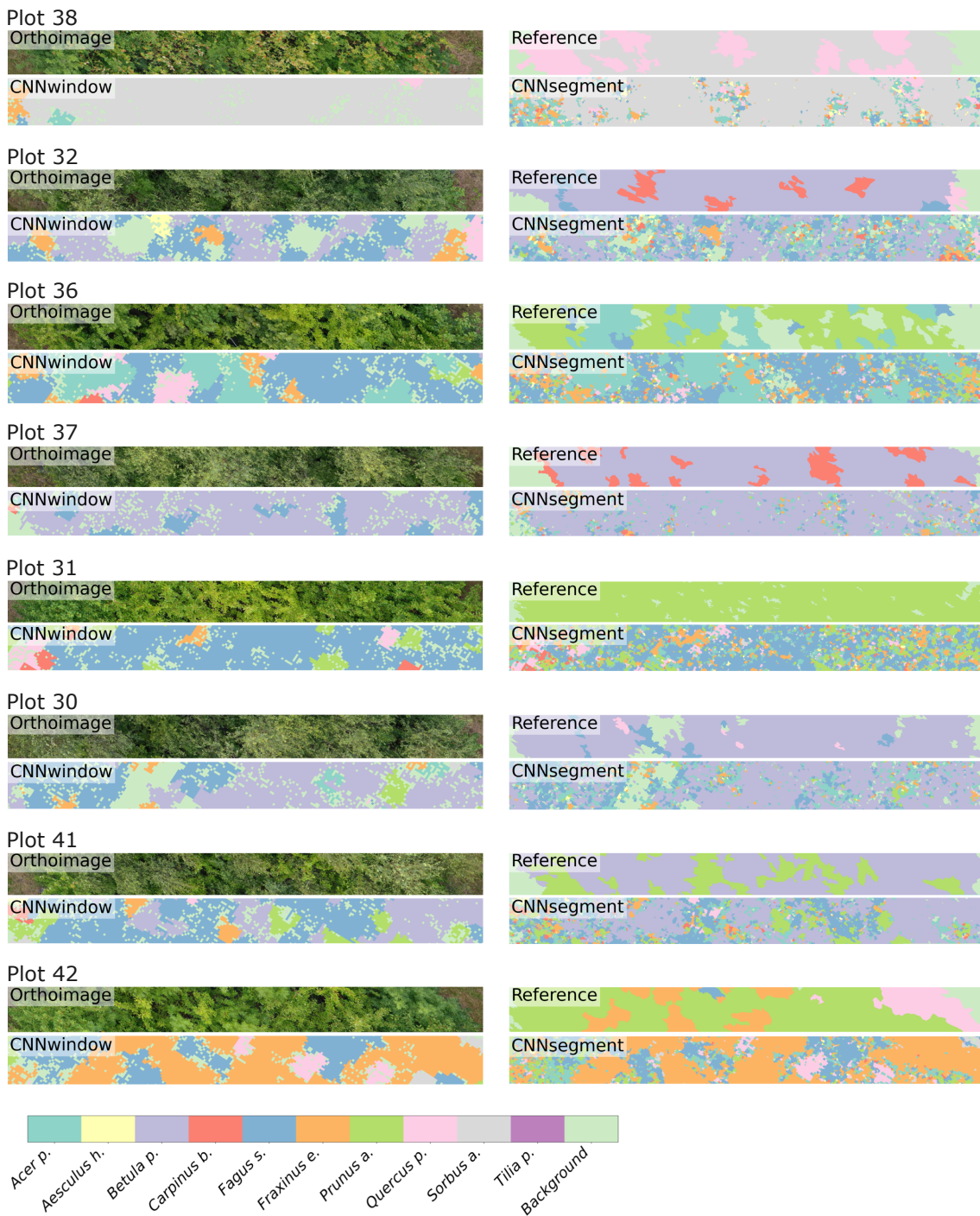


Figure A7: Transects of 2 m by 20 m of selected plots, including the orthoimage, the reference, CNN_{window} predictions, and CNN_{segment} predictions.

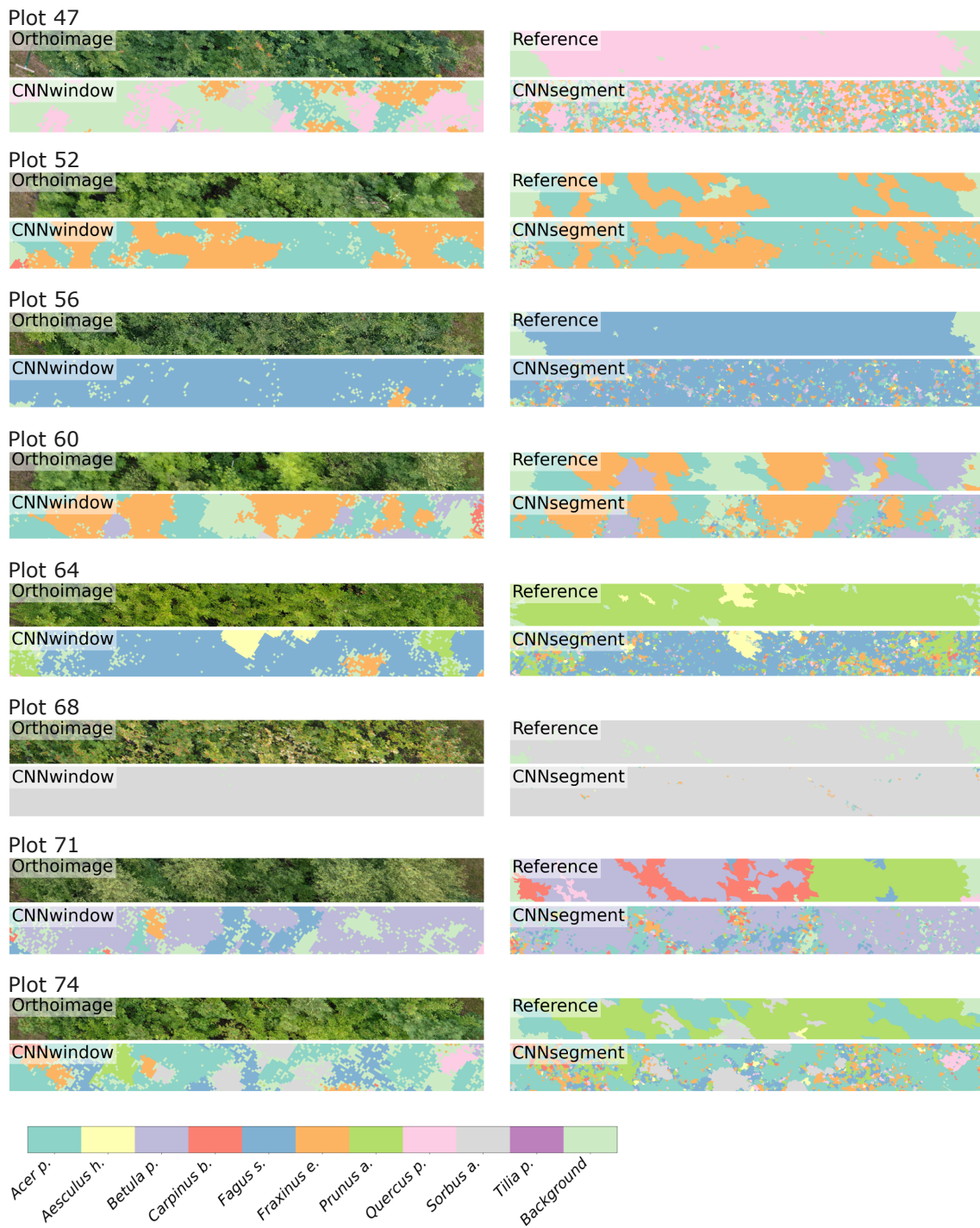


Figure A8: Transects of 2 m by 20 m of selected plots, including the orthoimage, the reference, CNN_{window} predictions, and CNN_{segment} predictions.

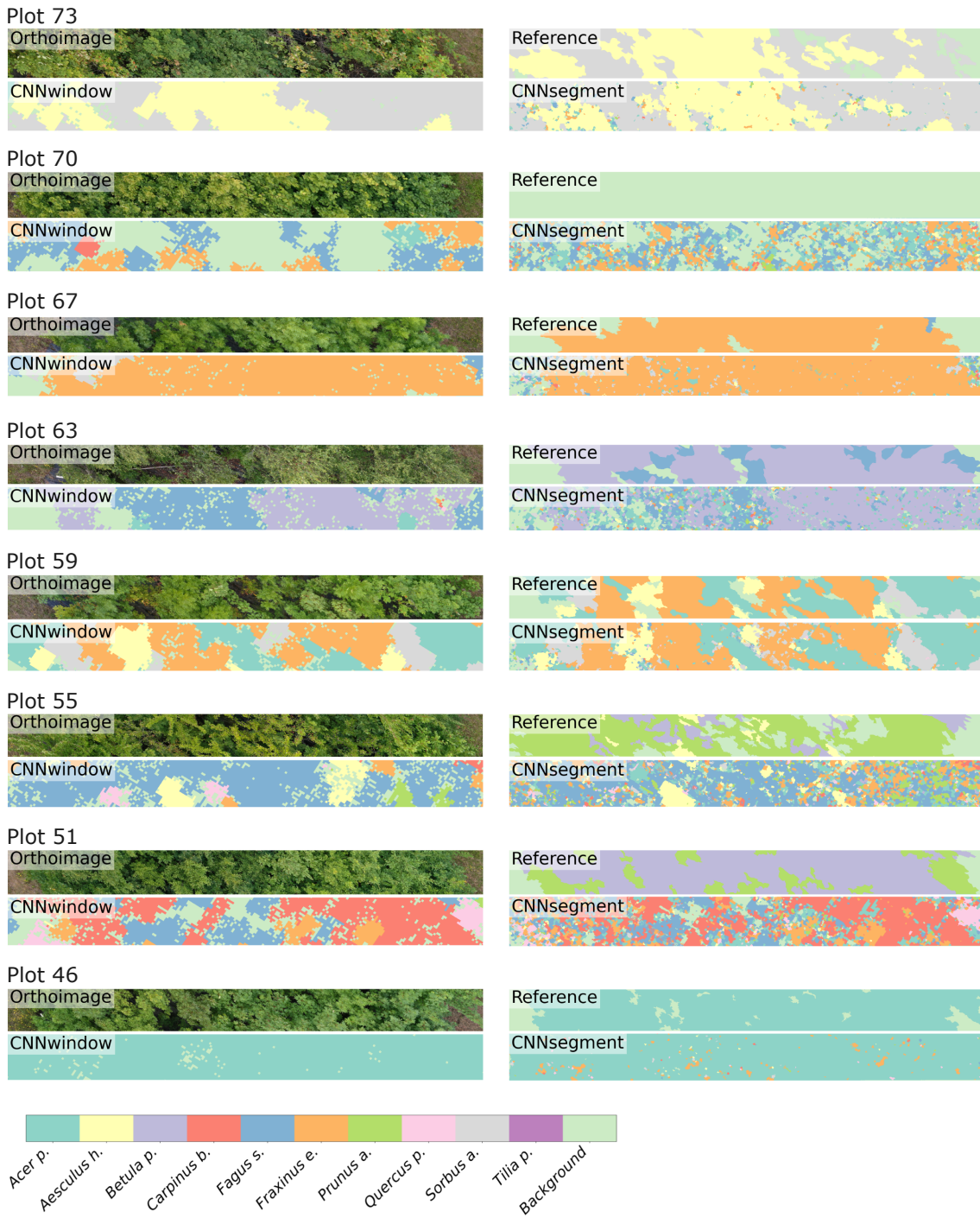


Figure A9: Transects of 2 m by 20 m of selected plots, including the orthoimage, the reference, CNN_{window} predictions, and CNN_{segment} predictions.

658 **A1.2 Confusion Matrix**

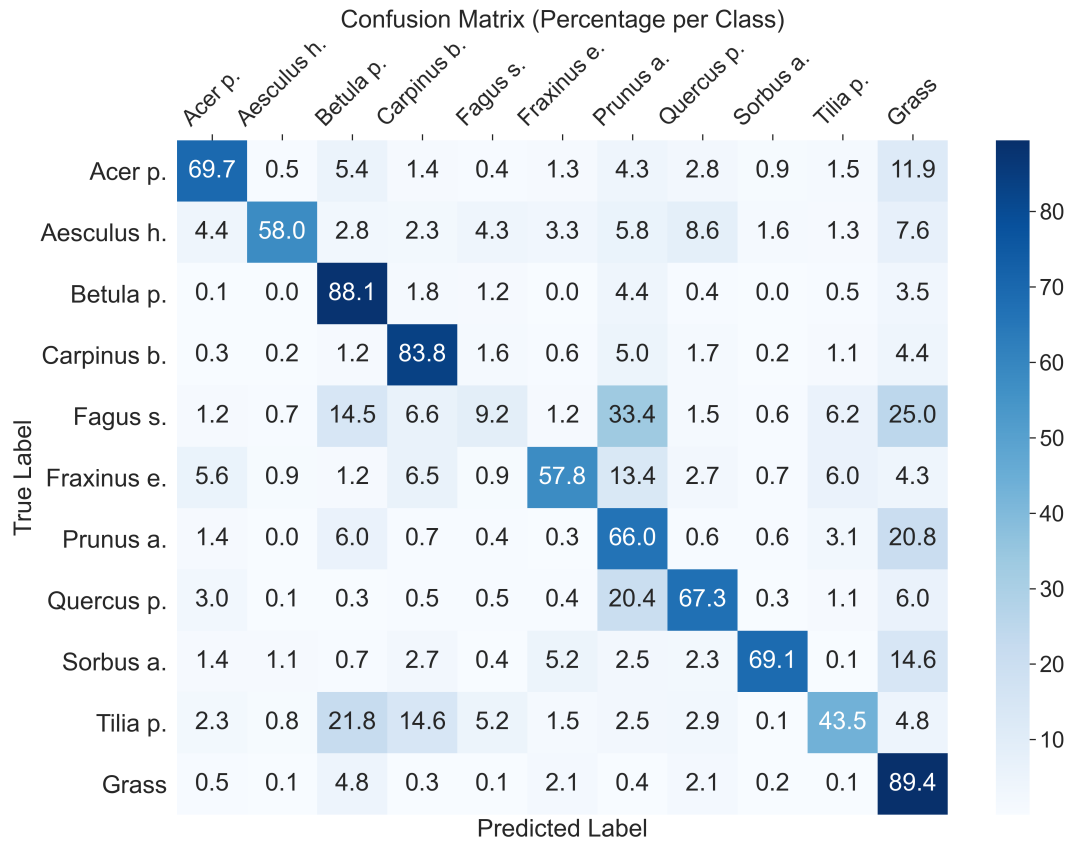


Figure A10: Normalized Confusion Matrix of the CNNsegment model applied to Ortho_{September}

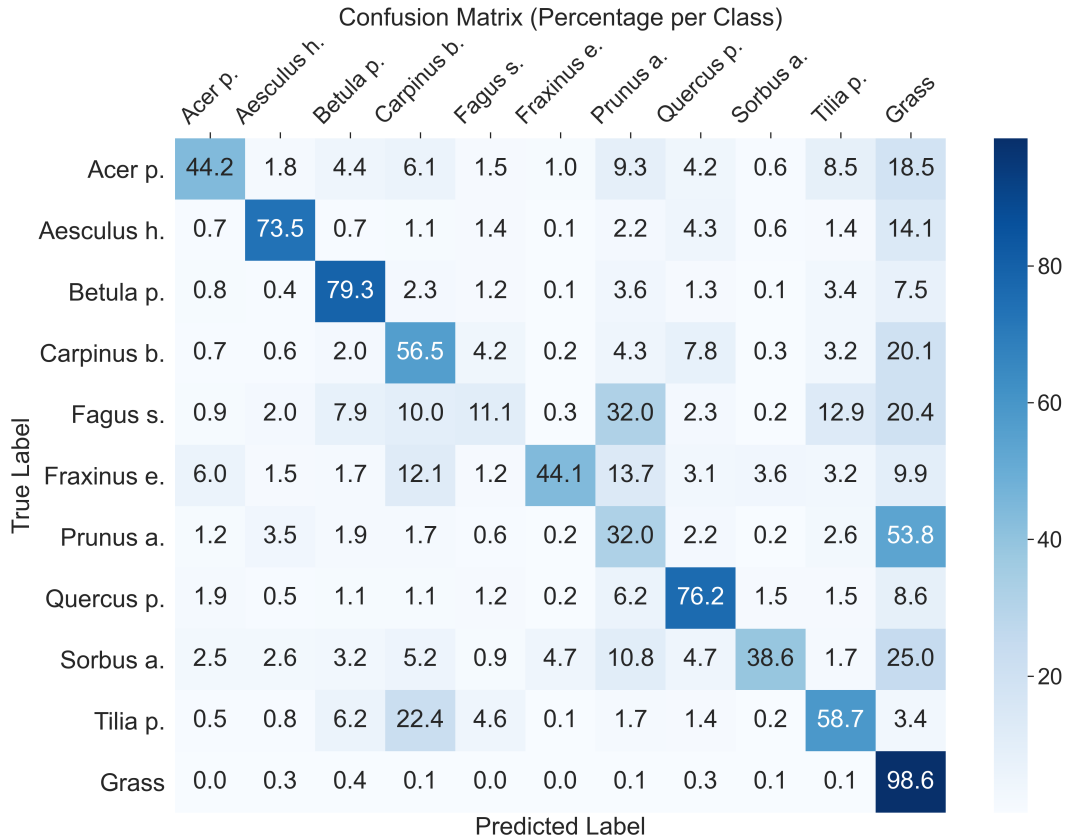


Figure A11: Normalized Confusion Matrix of the CNNsegment model applied to the Ortho_{September}

659 A1.3 Data pre-processing

660 To reduce the heterogeneity of crowd-sourced photographs and match them with the UAV
 661 perspective, we filtered the photographs based on their acquisition distance and plant leaf
 662 visibility. The model achieved an $R^2= 0.7$ and $F1 = 0.8$ on independent test data for both
 663 variables. Using predicted acquisition distance and tree trunk presence information for each
 664 photograph, we tested different filtering thresholds and combinations prior to training the
 665 CNN_{window} model for plant species classification. The best result was achieved by filtering
 666 photographs with acquisition distances outside the range of 0.3 to 15 m and excluding pho-
 667 tographs that showed tree trunks, with a probability of being a trunk > 0.5 .

668 **A1.4 Citizen science data availability**

Table A1: Number of downloaded photographs for selected tree species from the iNaturalist and Pl@ntNet datasets.

No.	Species	iNaturalist	Pl@ntNet
1	Acer pseudoplatanus	9999	3205
2	Aesculus hippocastanum	9998	1444
3	Betula pendula	9998	1308
4	Carpinus betulus	7165	2633
5	Fagus sylvatica	9981	3304
6	Fraxinus excelsior	7745	3130
7	Prunus avium	9999	3022
8	Quercus petraea	1491	221
9	Sorbus aucuparia	10000	2730
10	Tilia platyphyllos	582	1449

669 **A1.5 Segmentation model architecture**

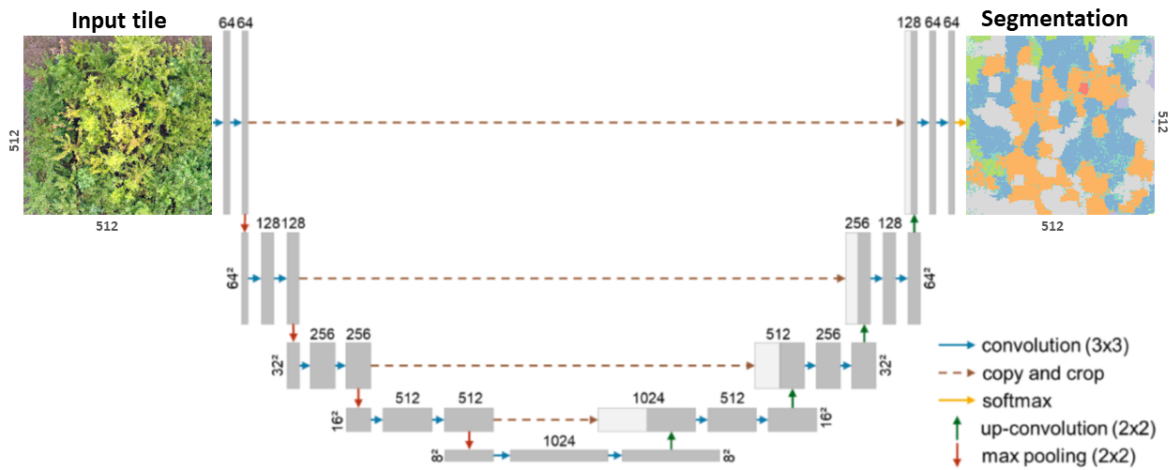
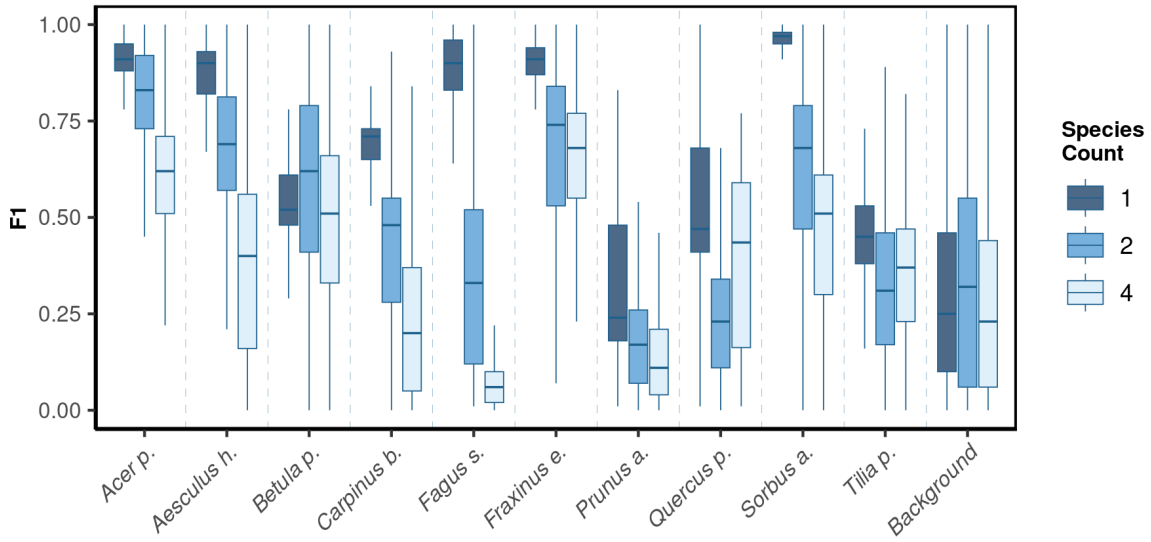
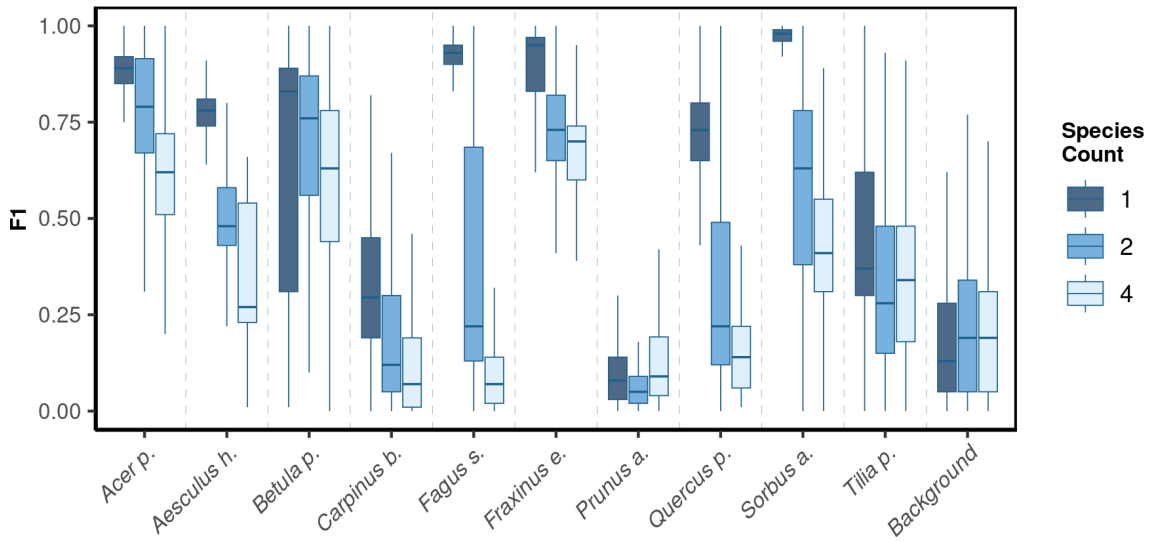


Figure A12: A modified version of the U-Net CNN-architecture for segmenting plant species from UAV orthoimages (Ronneberger et al., 2015).

670 **A1.6 CNN window species mixture box plot**



(a) Performance on Ortho_{July}: The model performance (F1) of the CNN_{window} model on Performance on Ortho_{July}.



(b) Performance on Ortho_{September}: The model performance (F1) of the CNN_{window} model on Performance on Ortho_{July}.

Figure A13: The model performance (F1) of the CNN_{segment} model across a gradient of canopy complexity in two orthoimages.